Source attribution of European surface O₃ using a tagged O₃ mechanism

Aurelia Lupaşcu[1] and Tim Butler[1,2]

[1]Institute for Advanced Sustainability Studies (IASS), Potsdam, 14467, Germany
[2]Freie Universität Berlin, Institut für Meteorologie, Berlin, Germany

Correspondence: A.Lupascu (Aurelia.Lupascu@iass-potsdam.de)

Abstract.

Tropospheric ozone (O_3) is an important air pollutant that affects human health, ecosystems and climate. The contributions of O_3 precursor emissions from different geographical source regions to the O_3 concentration can help to quantify the effects of local versus remote transported precursors on the O_3 concentration in a certain area. This study presents a "tagging" approach

5   within the WRF-Chem model that attributes O_3 concentration in several European receptor regions to nitrogen oxides (NO_x) emissions from within and outside of Europe during April-September 2010. We also examine the contribution of these different precursor sources to various O_3 metrics, and their exceedance events. Firstly, we show that the spatial distributions of simulated monthly mean MDA8 from tagged O_3 sources regions and types for late spring, summer and early autumn 2010 varies with season. For summer conditions O_3 production is dominated by national and intra-European sources, while in the late spring

10   and early autumn intercontinental transported O_3 is an important contributor to the total O_3 concentration. We have also identified shipping activities in the Mediterranean Sea as an important source of O_3 for the Mediterranean countries, as well as the main contributor to high MDA8 O_3 concentration, modelled in the Mediterranean basin itself. Secondly, to have a better understanding of the origin of MDA8 O_3 exceedances, we compare modelled and observed values of MDA8 O_3 concentration in the "Alps" and "Germany-Benelux" receptor regions, revealing that the contribution from local sources is about 45 % and

15   38 % of modeled MDA8 O_3 during the exceedances days respectively. By examining the relative contributions of remote NO_x sources to modelled and observed O_3 exceedance events, we determine that model underrepresentation of long-range O_3 transport could be contributing to a general underestimation of modelled O_3 exceedance events in the Germany-Benelux receptor region. Thirdly, we quantify the impact of local vs. non local NO_x precursors on O_3 production for each European receptor region using different O_3 metrics. The comparison between mean, MDA8 and 95th percentile O_3 metrics accentuate

20   the importance of large contributions from locally-emitted NO_x precursors to the high-end of the O_3 distribution. When we compare the vegetation and health metrics, we notice that the SOMO35 and AOT40 indexes exhibit a rather similar behaviour, while the W126 index accentuates the importance of local emissions. Overall, this study highlights the importance of a tagging approach to quantify the contribution of local and remote sources to the MDA8 O_3 concentration during several periods as well to different O_3 metrics. Moreover, this method could be applied to assess different mitigation options.

1 Introduction

Tropospheric ozone (O_3) is formed primarily through reactions of nitrogen oxides (NO_x) and volatile organic compounds (VOC) in the presence of sunlight. The World Health Organization air quality guideline (WHO, 2006, 2017) report that high O_3 concentrations can cause damages to humans and vegetation. It has been shown that the background O_3 concentrations have

5   increased during the last several decades due to the increase of overall global anthropogenic emissions of O_3 precursors (HTAP, 2010). Large cities are facing serious challenges in surface O_3 pollution due to urbanization and motorization processes (e.g. Chan and Yao, 2008). Moreover, it has been shown that tropospheric O_3 also affects radiative forcing (e.g. Ramaswamy et al., 2001; Stevenson et al., 2013) and therefore contributing to climate change. To maintain a good air quality and understand O_3's response to climate change, it is important to understand the contribution of different sources of its precursors (NO_x and VOC)

10   to the tropospheric O_3 concentration.

Emissions of NO_x and VOCs, as well as the emissions sources and weather conditions are important to understand the formation of the O_3 in the troposphere. The development of chemical transport models leads to a better understanding of the processes that contribute to high O_3 episodes and can help the authorities to develop strategies to reduce the impact of O_3 on both human well-being and ecosystems by knowing the impact of source emissions of NO_x and VOC such as surface

15   anthropogenic sources, fires, soil, and the stratosphere on total O_3 production. Several approaches have been used to determine the source attribution of O_3. For example, estimations of the changes in O_3 concentration have been made by perturbation of different emissions categories (e.g. Fiore et al., 2009).

Tagging techniques have also been used in modelling studies to determine source attributions for pollutants at given locations and source/receptor relationships. Pollutants with relatively low chemical reactivities such as carbon monoxide (CO) can be

20   "tagged" according to its emission sectors or regions for attribution studies (e.g. Pfister et al., 2011). Sudo and Akimoto (2007), and Derwent et al. (2015) used O_3 tracers tagged by their region of formation. They have found that the intercontinental transport of O_3 from polluted source region such as North America and East-Asia appears to be the most important source of tropospheric O_3 in Europe. The Wang et al. (2009) and Grewe et al. (2010, 2012, 2017) studies showed that the tagging method is used to identify contribution from individual sources due to its ability to track the emitted NO_x species during transport and

25   chemical processing. Moreover, Grewe et al. (2012) showed the impact of the tagging method on mitigation measures, while Dahlmann et al. (2011) studied the contribution of O_3 sources to O_3 radiative forcing. The studies of Emmons et al. (2012) and Butler et al. (2018) describe a procedure for tagging O_3 produced from NO_x sources through updates to the MOZART chemical mechanism. In addition, Butler et al. (2018) have extended the tagging technique to account for the VOC sources.

Based on Emmons et al. (2012) work, Pfister et al. (2013) and Safieddine et al. (2014) used the WRF-Chem regional model

30   to quantify the role of inflow (defined as source of O_3 and odd nitrogen species entering into a regional domain at the lateral boundaries) and of anthropogenic NO_x precursors on the surface O_3. Using a slightly different methodology, Gao et al. (2016) have employed within WRF-Chem a tagging based on Ozone Source Apportionment Technology (OSAT) (Yarwood et al., 1996) incorporated in the Comprehensive Air quality Model with extensions (CAMx).

Many efforts have been made to understand the origin of tropospheric O_3 and the key role played by the intercontinental transport, the contribution of stratospheric O_3 intrusion, and of different emissions sources to tropospheric O_3 concentration in a wide range of receptor regions. For a better understanding of these interactions, is necessary to know the relation between the amount of an emitted species and its atmospheric concentration. Thus we can quantify the contribution of different emission

5   precursor sources to the O_3 concentration at a receptor location. For this purpose, following Emmons et al. (2012) and Butler et al. (2018), we implemented into the regional WRF-Chem model a tagging technique that can be used to quantify the source contributions to the tropospheric O_3 concentration, by "tagging" emissions of NO_x, and corresponding resulting products and following them to the production of O_3.

Important objective when we are studying O_3 is its effect on humans and vegetation. Therefore, based on hourly aver-

10 aged data, several exposure indexes have been defined in order to describe the relationship between O_3 and human health and agricultural crop yield. Musselman et al. (2006), Agathokleous et al. (2018), and Lefohn et al. (2018) present a literature overview on O_3 metrics, while Paoletti et al. (2007) presents a list of common O_3 exposure metrics used to assess risk to human health and vegetation across Italy during the 2000-2004 period. Here we use some well-known O_3 metrics, such as MDA8, SOMO35, AOT40 and W126. The MDA8 index (Lefohn et al., 2018) is defined as the maximum daily av-

15 erage 8-h (MDA8) O_3 values (in units of ppb). SOMO35 (WHO, 2001) is determined by European protocols (EU directive 2008/50/EC, 2008) and it is defined as the annual sum of MDA8 O_3 with a cut-off of 35 ppb, The AOT40 and W126 vegetation metrics have been used in air pollution regulation in Europe (EU directive 2008/50/EC, 2008) and the United States (U.S. EPA regulations https://www.gpo.gov/fdsys/pkg/FR-2015-10-26/pdf/2015-26594.pdf). In the European legislation (EU directive 2008/50/EC, 2008), the AOT40 metric is accumulated over the daytime period from May to July and it has a defined

20 target limit of 18000 $\mu g\ m^{-3}$ h (9000 $ppb - hours$) and a long term objectives of 6000 $\mu g\ m^{-3}$ h (3000 $ppb - hours$). A standard of 15 $ppm - hours$ is defined for the seasonal W126 index averaged over three years. Lefohn and Musselman (2012, https://www.fcpotawatomi.com/wp-content/uploads/2015/01/Vegetation.pdf) stated that the W126 index "... would provide a more appropriate target for air quality management programs designed to reduce emissions from anthropogenic sources contributing to O_3 formation". These metrics have been used side by side to assess the impact of mitigation strategies (Avnery

25 et al., 2013), the impact of industry on air quality management issues (Vijayaraghavan et al., 2016), and the impact of high O_3 levels and temperatures on crops (Tai and Val Martin, 2017).

In this paper we use a tagged O_3 mechanism in the WRF-Chem regional chemistry-climate model to understand the contributions of O_3 precursor emissions from different geographical source regions on the modelled O_3 concentration in several European receptor regions. In Section 2 we briefly describe the details of the implementation of this tagging technique point-

30 ing to the changes made to both the chemical mechanism and WRF-Chem code. Section 2 also provides a description of the WRF-Chem configuration, simulation design, and input data used in the study. An analysis of the WRF-Chem simulations is presented in Section 3, while Section 4 summarizes our findings.

2   Model simulation

2.1   Tagging technique

In order to implement a tagging approach, several changes must be implemented in the model code to accommodate additional tracers and reactions representing tagged constituents. Butler et al. (2018) describes in detail how the tagging technique was

5   implemented in the Community Earth System Model. The tagging technique used in this study is based on the same approach, and uses the same modified version of the MOZART chemical mechanism. Further detail on how the chemical mechanism was extended can be found in Butler et al. (2018).

In order to use the NO_x tagging mechanism, a new chemistry option was added in the namelist.input file: chem_opt=113 as through the code. The coupling of the new chemical scheme with microphysics and radiative processes requires several

10   modifications to code: 1) The first step is to create a new chemistry option. The package mozart_tag_kpp (chemopt==113) has been added to /Registry/registry.chem together with new model variables for tagged NO_x species, for example, O3_X_INI, O3_X_STR, etc. For this purpose, the pre-processing software described in Butler et al. (2018) was adapted in order to produce a new chemical mechanism; 2) The new chemistry package is a KPP option. Therefore, we created a new subdirectory in /chem/KPP/mechanisms/ directory containing the files (*.spc, *.eqn, *.kpp, and *.def) which defined the chemical model

15   species and constants, chemical reactions in KPP format, model description, computer language, precision, and integrator.

The KPP chemical preprocessor, version 2.1 (Sandu and Sander, 2006) used by WRF-Chem has an upper limit of the numbers of species and reactions in the chemical mechanism. Thus, the header file gdata.h, located in /chem/KPP/kpp/kpp-2.1/src, has been modified to enable to model capacity to be used for a large number of species and reactions.

Further, we updated the subroutines in the chem directory to take in account these packages. The modules that we modified

20   are described in the Appendix.

Although WRF-Chem uses the Advanced Research WRF (ARW) dynamic core in this simulation which conserves mass and scalar mass (Grell et al., 2005), the tagged O_3 species are advected independently. Thus, numerical errors associated with the advection scheme led to gradients in the sum of tagged species concentration compared to the "real" concentration; therefore the relationship between these variables is not conserved. Since the advection scheme fails to reproduce the expected solution

25   (in which the sum of the tagged species concentration at each grid point must be equal to "real" concentration), we solve this by fixing all undershoots and/or overshoots assuming that the sum of tagged species mass is proportional to the "real" concentration. This technique was also applied in Flemming et al. (2015), and Gromov et al. (2010).

Compared to Pfister et al. (2013) and Safieddine et al. (2014) work, the expanded tagging technique used in this study has the advantage that multiple tags can be defined in each model run.

30   2.2   Experiment setup

WRF-Chem version 3.7.1 was used for this study to account for the impact of different global and European O_3 precursor source regions to several European receptor regions during the April-September 2010 period. A single domain, that covers the area between 32° N and 70° N, and 29° W and 57° E, was used with 50-km grid spacing and 35 vertically-stretched layers from

the ground up to 50 hPa. The physics options used for this study include the Morrison double-moment microphysics scheme (Morrison et al., 2009), the Grell-Freitas cumulus parameterization (Grell and Freitas, 2014), the Rapid Radiative Transfer Model (Iacono et al., 2008) for longwave and Goddard shortwave scheme (Chou and Suarez, 1994), the Yonsei University boundary-layer parameterization (Hong et al., 2006), and the Monin-Obukhov scheme for the surface layer (Jiménez et al.,

5   2012).The initial and boundary conditions for meteorological fields are using the European Centre for Medium-Range Weather Forecasts (ECMWF) reanalyses. Anthropogenic emissions were obtained from the TNO-MACC III emission inventory for Europe (Kuenen et al., 2014). Because the model domain extends beyond the edges of TNO-MACC III inventory, we used for completion emissions from the HTAP V2 inventory (http://edgar.jrc.ec.europa.eu/htap_ v2). Biogenic emissions were computed on-line using the Model of Emissions of Gases and Aerosols from Nature (MEGAN) model (Guenther et al., 2006). The

10   biomass burning emissions are based on Fire INventory from NCAR (FINN) (Wiedinmyer et al., 2011).

    For this WRF-Chem simulation, the tagged MOZART chemical mechanism for NO_x emissions (Butler et al., 2018) is used to represent the gas-phase chemistry. The photolysis rates were computed using the Fast Tropospheric Ultraviolet and Visible (FTUV) Radiation Model (Tie et al., 2003; Li et al., 2005). The dry deposition was calculated following the Wesely (1989) resistance method, while the wet removal scheme for the tagged MOZART chemistry is based on Neu and Prather (2012).

15   In order to represent the impact of transported O_3 from different regions outside of the domain, for the trace gases we used boundary conditions derived from the extended CAM-Chem version 1.2 global simulations. Butler et. al (in preparation) used the tagging approach within the CAM-Chem model for several HTAP2 source regions such as: ASI (Asia), NAF (North-Africa), NAM (North-America), OCN (Oceanic sources), RBU (Russia, Belarus, Ukraine), and RST (rest of the world), as well as for several source types: BIO (biogenic emissions), BMB (biomass burning emissions), LGT (lightning), and STR

20   (stratospheric O_3). Using a division of source/receptor regions within the European model domain, we define 15 geographical regions for this study, as shown in Figure 1 and Table 1. Source regions within the European domain are identical to European receptor regions in our study. A similar division of European regions has been used by Christensen and Christensen (2007) and Otero et al. (2018) to address the main sources of uncertainty in regional climate simulations, as well as during the AQMEII project (i.e. Struzewska et al., 2015).

25   For each receptor region we analyse the impact of the anthropogenic NO_x emissions coming from different source regions to the total O_3 concentration. The BIO, BMB, LGT, and STR types are also included in the simulation, but without including them into the division of source/receptor regions.

2.3   Ozone metrics

By the means of different O_3 impact metrics we determinate which are the most important O_3 precursor sources for different

30   kinds of O_3 impact in different receptor regions, and thus to provide insight into appropriate mitigation measures. These metrics include the mean O_3 concentration, the mean of the maximum daily 8-hour O_3 (MDA8), the cumulative exposure to mixing ratios above 35 ppb (SOMO35) (Colette et al., 2012), and the 95th percentile for surface O_3, the impacts of O_3 exposure on trees, plants and ecosystems (W126) (Lapina et al., 2014), the AOT40 accumulation metric (the threshold is 40 ppb) were used to assess risk to vegetation from O_3 exposure (UNECE, 2010).

The European Air Quality Directive (EU directive 2008/50/EC, 2008) defines a target value of 120 μg m^{-3} for the MDA8 concentration, which can be exceeded up to 25 days per calendar year averaged over three years. The modeled daytime AOT40 (during local daylight hours 8 AM – 7 PM) was calculated according to Equation (1).

$$AOT40 = \sum_{i=1}^{90 \text{ days}} \left(\sum_{h=8}^{19} max\left(O_{3i,h} - 40,0\right) \right) \tag{1}$$

5 According to the European legislation (EU directive 2008/50/EC, 2008), the AOT40 metric is accumulated over the daytime period from May to July and it has a defined target limit of 18000 μg m^{-3} h (9000 ppb $-$ hours) and a long term objective of 6000 μg m^{-3} h (3000 ppb $-$ hours). W126 is calculated according to U.S. EPA regulations (https://www.gpo.gov/fdsys/pkg/FR-2015-10-26/pdf/2015-26594.pdf). A standard of 15 ppm $-$ hours is defined for the seasonal W126 index averaged over three years. For this study, the hourly surface O$_3$ tagged outputs for April through September are used to calculate the highest

10 3-month W126 (see Eq. 2):

$$W126 = \sum_{i=1}^{90 \text{ days}} \left(\sum_{h=8}^{19} O_{3i,h} \cdot \left(\frac{1}{1 + (4403 \cdot e^{-126 \cdot O_{3i,h}})} \right) \right) \tag{2}$$

According to Lefohn et al. (1988), the W126 index includes all hourly O$_3$ values within the specified time range, although a lower weight is given to hourly O$_3$ concentrations bellow the inflection point at 65 ppb, whilst above 90 ppb the weighting factor is almost 1. SOMO35 (WHO, 2001) is defined as the sum of the MDA8 O$_3$ with a cut-off of 35 ppb (see Eq. 3). For this

15 metric, the EU air quality directives do not prescribe a limit or a target values.

$$SOMO35 = \sum_{h=1}^{6 \text{ months}} max\left(MDA8_i - 35,0.0\right) \tag{3}$$

The contribution of tagged O$_3$ concentration to each metric is calculated from the model output based on metric formulations. In the case of MDA8 and 95th percentile metrics, we search for the specific period when the calculated values for total O$_3$ concentration meet the requirements given by formulation of these metrics. Once this is identified, the tagged O$_3$ concentrations

20 are extracted for the same period which are then used further in our analysis. However, the contribution of these tagged O$_3$ concentrations to the cumulative metrics is slightly different and it uses proportion of each tagged species to the total O$_3$, as illustrated below for AOT40 at specific hour:

$$AOT40_{tag} = \sum_{i=1}^{90 \text{ days}} max\left((O_3 - 40.) \cdot \frac{O_{3,tag}}{O_3}, 0.0 \right) \tag{4}$$

Based on their formulation, we grouped these metrics in non-cumulative (mean O$_3$, MDA8, and the 95th percentile) and

25 cumulative (SOMO35, W126, and AOT40) categories. Since these metrics have different formulation (using hourly O$_3$ values of O$_3$ values above a threshold) and they do not cover the same period of time, to facilitate a more direct comparison between metrics, an analysis of the relative contribution of different source regions to the total O$_3$ in each receptor region using different O$_3$ metrics is done using averaged values for non-cumulative metrics, 6-months sums for SOMO35, AOT40 calculated for crops (cumulated over May-July period) and maximum of 3-months sums for every consecutive 3-months period for W126 index.

3 Results and discussions

The discussion of the model results focuses on the April-September 2010 period. We first briefly evaluate the ability of WRF-Chem to reproduce the meteorological parameters using measurements from the Global Weather Observation (GWO) dataset provided by the British Atmospheric Data Center (BADC), and observed O_3 concentration using the measurements included in the AirBase European air quality data base (EEA, 2017). We then provide a more detailed analysis of the contribution of the different source regions and types to the MDA8 total O_3 for the analysed period.

3.1 Evaluation of meteorology and chemistry

Since the accurate simulation of meteorological parameters represents a key factor that affects the trace gases concentration, we briefly compare the modelled mean sea level pressure (MSLP), 2 m temperature (T2M), 10 m wind speed (WS10M) and direction (WD10M) variables against the GWO measurement. Predicted model variables are evaluated against observations using statistical scores that include normalized mean bias (NMB), and correlation factor between simulated and measured values (r).

An extensive evaluation and discussion of the long term meteorological and O_3 model performance of WRF-Chem using the MOZART chemical mechanism has been presented by Mar et al. (2016). Due to the coarse resolution of the domain that will not properly reproduce the air parcel dynamics associated with the complex topography in the mountainous areas, we assess the ability of the model to reproduce the meteorological variables using only those measurements sites located bellow 1500 m above ground level. MSLP is well reproduced at European scale over the entire period (NMB of 0 % and r of 0.98). In terms of spatial correlation, T2M performs very well (r = 0.91), however the observed temperature is underestimated by 3 % (see Table 2). WS10M is fairly well reproduced both in terms of spatial and temporal variability (NMB = 8 %, r = 0.63). Yet, WD10M did not perform as well as the other meteorological variables (NMB = 13 %, r = 0.47) and this behavior could be related to unresolved topography features (Jimenez and Dudhia, 2012). Also, the model performance is similar to Mar et al. (2016) and Tuccella et al. (2012).

We also compare the modelled MDA8 O_3 concentration against observations provided by the publicly available AirBase dataset. The relatively coarse resolution of the domain might not be representative for the changes in the local emissions when the measurements are representative for urban condition; therefore further for the analysis we use only those stations characterized as rural background. As can be seen from Table 3, the model evaluation over the whole period shows that both tests perform quite well in terms of concentration (NMB = -5.2 %) and temporal evolution (r = 0.69). Mar et al. (2016) reported a mean bias (MB) of 15.85 μg m^{-3} and NMB of 17 % for the June-August 2007 period when the MOZART mechanism was used to assess the chemical performances of the model, whereas for the same period we obtain a MB of -5.92 μg m^{-3} and a NMB of -6.3 %. Tuccella et al. (2012) reported an annual MB of -1.4 μg m^{-3} when the RADM2 chemical mechanism was used to simulate the year 2007. Month-to-month analysis (Table 3) shows the model reproduces the O_3 concentration well compared to the Mar et al. (2016) and Tuccella et al. (2012) studies. Even though the model performance in terms of temporal variation is relatively good (r between 0.58 and 0.71), it mostly underestimates the observed concentration, except in September when the

model overestimates the observed concentrations (NMB = 4.6%). The modelled errors could be explained by a wide range of uncertainties related to the modelled physical and chemical processes such as grid resolution, vertical and horizontal transport, boundary layer mixing, emissions inventory, chemistry and photolysis rates, dry deposition and wet scavenging, etc as well as uncertainties in the measurements. As the focus of this study is on the contribution of different O_3 sources and of its precursors

5   to the tropospheric O_3 concentration in a certain area, a more thorough analysis of the model ability to reproduce the observed meteorological variables is beyond the scope of this paper.

3.2   Contribution of tagged precursor sources to the MDA8 O_3 concentration

Figure 2 shows the spatial distributions of simulated monthly mean MDA8 from tagged O_3 source regions and types for late spring 2010. The receptor regions are mainly influenced by the overseas combination of NAM, ASI, OCN, and RST sources

10   that together have a contribution varying from 25 % in the ALP region (that include Po Valley, characterized as one of the most polluted areas in Europe); up to 53.6 % in the UKI region (see Table S1). O_3 from RST (7.5 - 15 % contribution) is the main overseas source. The O_3 coming from oceanic sources affects mostly the Atlantic coastal countries (up to 16.1 % contribution in the UKI region), yet a small contribution of ~4-5 % can be seen over the inland regions. The long-range transported O_3 from Asia and North America contributes from 9.6 % in ITA and up to ~22 % in UKI and SCA. After intercontinental transport,

15   the O_3 produced elsewhere in Europe is an important source of O_3 in the receptor regions, followed by O_3 coming from other types (LGT, BIO, and BMB). In general, for this time of the year, the contribution from the local sources to the total MDA8 O_3 concentration in the receptor regions is within a range from 8.5 % (SCA) to 21 % (RBU) (see Table S1). In all receptor regions, the MDA8 O_3 concentration is dominated by O_3 produced by remote anthropogenic precursors, consistent with previous work, i.e. Fiore et al. (2009) and Li et al. (2016). Using observations, Danielsen (1968), Thouret et al. (2006)

20   showed that the transport from the stratosphere contributes to tropospheric O_3. Here, the stratospheric O_3 contributes up to 7 ppb (12.5 % in SCA) to the total MDA8 O_3 concentration, similar to Derwent et al. (2015). A similar tagged system, but for the CAM-Chem model (Butler et al., 2018), also shows that the stratospheric O_3 has a large contribution to the total tropospheric O_3 concentration. The MOZART chemical mechanism used in this study does not explicitly treat the stratospheric chemistry; thus the surface stratospheric O_3 could be attributed to the vertical and horizontal transport of stratospheric O_3 coming from

25   the boundary conditions. The emitted local sources do not only affect local O_3 concentrations, but they also impact the O_3 levels of bordering countries due to a strong horizontal pollution transport.

During June-August 2010, Western Europe was mostly influenced by a high-pressure systems centered over the Atlantic (see Fig. S1). In the upper troposphere, a ridge influenced the vertical structure, especially over southern Europe. Therefore, these "usual summer conditions" favoured the intrusion of warm air coming from Africa and the Arabic Saudi peninsula and

30   led to a warm and dry climate characterized by subsidence, stability, clear sky and high solar radiation intensity. Hence, the photochemical O_3 formation is enhanced, leading to a stronger contribution from local emissions to the total concentration compared to the previous period. Figure 3 depicts the average MDA8 O_3 for June-August 2010. For most regions, we notice an enhancement of O_3 produced from local sources in June-August compared with April-May (Figure 2). Local sources can contribute more than 20% to the mean MDA8 O_3 concentration (from 14.6 % in SCA to 33.6 % in ALP, see Table S1),

showing that the local sources play a stronger role in O_3 formation during the June-August period, as previously shown by Jiménez et al. (2006) and Querol et al. (2018). Compared with late spring, the relative contribution of the overseas sources decreased in summer, varying from 12.8 % in the ALP receptor region to 44.8 % in the UKI region in July (see Figs. 2, 3 and Table S1). We notice a reduced spread of O_3 produced from European anthropogenic precursors over the bordering regions

5   compared with late spring 2010 (see Figs. 2 and 3). The increase in average temperature combined with stable atmospheric condition lead to an enhancement of the biogenic NO emitted in the atmosphere, especially in South-Eastern and Eastern Europe; thus the BIO source type contributes up to ~9 ppb (13.2 % of MDA8 O_3) in the RBU receptor region (see Fig. 3). The vegetation fires that took place across Russia in July and August (Gilbert, 2010; Huijnen et al., 2012) as well as in Portugal and Spain (European Commission, 2011) lead to a contribution of O_3 coming from BMB up to 29 ppb (16 %) in the RBU

10   receptor region and up to 8.5 ppb (2.3 %) in the IBE receptor region. The BMB emissions contribute domain wide more than 3.6 % (ALP), the most affected receptor regions being RBU, IBA, SEE, SCA, and TCA. Another consequence of enhanced photochemical activity during the summer season is the reduction of stratospheric O_3 that contributes in general up to ~3-4% of total O_3 concentration at the surface.

     The decrease of the photochemical activity in September 2010 is reflected in the decrease of total O_3 concentration compared

15   with the summer season, as well as in the reduction of local source contribution to the total O_3 concentration (see Fig. 4). Thus, only in IBE, TCA, FRA, ALP and RBU region the contribution of local sources to total MDA8 O_3 is higher than 20 % (Table S1). On the other hand, we notice an increase in O_3 coming from overseas anthropogenic sources and lightning in autumn, stressing the seasonal variation in the outflow from other continents, and the variation in the lifetime of O_3 which is shorter during the summer due to the enhanced photolytic sink.

20   Although we have seen that long range transport plays a major role to O_3 concentrations, the tagging technique helps to gain more insights into which region of the world dominates these concentrations in spring or autumn. In early fall, the western European receptor regions exhibit a slight increase by of 1.6 % of O_3 concentrations coming from North-America compared with the spring season, whilst the contribution of O_3 concentrations coming from the other overseas sources to the total O_3 decreases. This could be linked to the prevailing westerly wind, and the synoptic conditions seen during the first period of

25   September, when the Azores High extended far to east and north (Fig S1), creating such conditions that direct transatlantic transport of American pollution can be seen far east. For example, in the RBU receptor region, the North-American and oceanic sources contribute up to 14.6 % in spring and 11.4 % in autumn to MDA8 O_3 concentration.

     Apart from local and other type sources, the NO_x emissions from shipping activities in the Atlantic Ocean combined with the oceanic O_3 from boundary conditions are an important source of O_3 that explains up to 16 % in late spring, 21% in summer

30   and 12% in early autumn of the MDA8 O_3 concentration in the UKI, IBE, FRA, GEN, CEN and SCA. Our results are similar to those presented by Tagaris et al. (2017) and the references therein, and Mertens et al. (2018) who showed that OCN contributes up to 20 % of total O_3 in the North Atlantic. Butler et al. (2018) showed that O_3 from oceanic sources reach a minimum in the North Atlantic Ocean during the summer, yet this study shows that in the UKI, IBE, FRA, GEN, CEN and SCA receptor regions the oceanic O_3 peaks its maximum contributions in the summer. This implies that the nearby shipping emissions have

35   a greater contribution in these oceanic bordering countries rather than oceanic O_3 from the boundary conditions. Furthermore,

the NO$_x$ emissions from shipping activities in the Mediterranean and Black Seas contribute up to 14 % in late spring, 19 % in summer and 11 % in early autumn of the MDA8 O$_3$ concentration predicted in the receptor regions situated along the shore of the Mediterranean Sea, such as IBE, ITA, SEE, ALP and FRA.

As can be seen from Figs. 2-4, the highest MDA8 O$_3$ concentrations are predicted over the Mediterranean basin due to the

5 several more favorable conditions for its formation like small deposition sinks and intense photochemistry. Several studies, such as Safieddine et al. (2014), Tagaris et al. (2017), Querol et al. (2018) and the references therein, have used source attribution methods to establish the origin of tropospheric O$_3$ observed over the Mediterranean Basin. The tagging technique used here shows that the O$_3$ from shipping activities in the Mediterranean and Black Seas (MBS) explains, on average, 15 % in late spring, 20 % in summer and 12 % in early autumn of total MDA8 O$_3$ predicted in the MBS receptor region, similar to Aksoyoglu

10 et al. (2016) that showed these emissions contribute within a range of 10 to 20 % to the mean O$_3$ in the Mediterranean in the summer of 2006. Moreover, Tagaris et al. (2017) shows that shipping emissions explain up to 30 % the MDA8 O$_3$ simulated for July 2006 over the Mediterranean Sea. This study shows that the shipping activities contribute up to 35 % to the MDA8 O$_3$ near the Strait of Gibraltar (see Figure 5) during thr April-September 2010 period. The shipping emissions have the highest contribution to the Western Basin of the Mediterranean Sea. Aside from shipping activities, the other European source regions

15 have a localized contribution to total MDA8 O$_3$ predicted in the Mediterranean Sea. Thus, ITA, ALP, GEN source regions contributes mostly to the central basin; IBE and FRA are main contributors in the western basin and SEE and TCA in the eastern basin. Natural sources contribute on average up to 10% of MDA8 O$_3$ in the western basin, and up to approximatively 25 % of MDA8 O$_3$ in the eastern basin. The long range transport contributes up to 45 % along the North African shore and it exhibits a zonal pattern, with low concentrations in the North and high concentrations in the South of the Mediterranean Sea,

20 mostly due to O$_3$ concentrations from NAF and RST sources.

3.3 Tagged ozone precursor contributions to exceedances of MDA8 target values – case study

As previously mentioned, the European Air Quality Directive (EU directive 2008/50/EC, 2008) has defined a target value of 120 μg m^{-3} for the MDA8 O$_3$ concentration, which can be exceeded up to 25 days per calendar year averaged over three years. In the following we call exceedances the values that surpass 120 μg m^{-3}, and non-exceedances the values below 120

25 μg m^{-3}. Figure S2 shows the spatial distribution of the number of exceedances observed and calculated throughout the April-September 2010 period for the AirBase rural stations. The observed MDA8 O$_3$ exceeds the target limits locally in Po Valley, Austria, Germany and the coastal area of Portugal, Spain, France and Italy and isolated in Poland, and Slovakia. Yet, the modeled exceedances do not exhibit the same spatial pattern or intensity as observed. Our use of tags allows the identification of main source contributors to exceedances of modelled MDA8 O$_3$. Given the high number of stations that measure O$_3$, for

30 simplicity, we will discuss the source contribution to the MDA8 O$_3$ exceedances only for the ALP and GEN receptor regions.

Figure 6 exhibits the contribution of each tagged source and type to the modeled MDA8 O$_3$ as well as the observed MDA8 O$_3$, samples in all cases at the location of the measurement stations, during the April-September 2010 period. Figure 6 shows averaged conditions during exceedance of the MDA8 target value, and also at times during which the target value is not

exceeded. In order to perform the source attribution for the observed values, we have scaled these values proportionally by the relative concentrations of each tagged O$_3$ tracer in our model output.

The relative contribution of emissions from different source regions to the modelled MDA8 O$_3$ and to the observed MDA8 O$_3$ scaled by the contribution of modeled sources of O$_3$ types is generally similar for both regions (see Fig. 6). In the ALP,

5 we can clearly pinpoint the main remote contributor is MBS (see Fig. 6), followed by GEN, and FRA, suggesting a dominant westerly and northerly flow. The recirculation of air masses in the Gulf of Genoa could accentuate the sea breeze and therefore more O$_3$ coming from NO$_x$ precursors associated to shipping activities in the Mediterranean will be transported to the coastal and inland station.

In GEN, the main remote source regions are FRA and CEN during the exceedance days and FRA and UKI during non-

10 exceedance days (Fig. 6). Opposite to ALP, in GEN the model predicts less MDA8 exceedances days. Comparing the source contribution to both modeled and observed exceedances days, we notice that model underestimates the O$_3$ concentration associated to the long range transport and natural sources and predicts more O$_3$ from CEN and FRA than observed. Underestimation of long-range transported O$_3$ into the GEN region in our model could be an explanation for the fact that the number of modeled MDA8 O$_3$ exceedances in GEN is half of the observed number of exceedances (Figure 6).

15 This kind of analysis can be applied to improve our knowledge of O$_3$ precursor's origin and their contribution to MDA8 O$_3$ health metrics. Hence, by the means of the tagging technique, the policy makers can identify future action required to control the NO$_x$ emissions at local and regional levels.

3.4   Tagged ozone precursor contributions to regulatory ozone metrics

In this section, we discuss the contribution of O$_3$ concentrations from diverse emissions sources and types to several different

20 metrics which quantify O$_3$ exposure of humans and ecosystems. From modelled hourly concentrations of tagged O$_3$ sources and types, we have calculated different O$_3$ metrics, such as non-cumulative (mean, MDA8, and the 95th percentile O$_3$) and cumulative (SOMO35, W126, and AOT40) metrics. We have chosen not to analyse the performance of the calculated cumulative metrics in comparison with the measurements, following previous work by Tong et al. (2009). Their work showed that the poor performance of the cumulative metrics is closely related to the sensitivity of these metrics to the threshold values or

25 weighting factors.

Figure 7 and Table S2 exhibit the percent contribution of different emissions sources and types to total O$_3$ as calculated for health and vegetation metrics. The non-cumulative O$_3$ metrics employed in this study have a similar pattern for most of receptor regions: the contribution of local and European sources to the total O$_3$ concentration is low when we apply mean O$_3$ metric and high when we are looking at 95th percentile, emphasizing the importance of O$_3$ produced by local and neighbouring

30 sources to the high end of the O$_3$ concentration distribution.

Splitting the non-cumulative metrics into early (April-June) and late (July-September) simulation periods clearly illustrates that the European receptor regions are more prone to being influenced by the intercontinental transport during early period than during late period. The intercontinental transported O$_3$ contribution to mean O$_3$ in different receptor regions is higher during theearly period and it spans between 22.8 % and 54.3 %, and it contribute between 16 % and 48.9 % during the

late season (see Fig. 7 and Table S2). Since in this case the O_3 associated with intercontinental transport is coming solely from boundary conditions, it implies that errors in boundary conditions affect the predicted concentration of various chemical species, consequently the contribution of the overseas sources to European O_3 (Tang et al., 2007; Giordano et al., 2015; Im et al., 2018).

5   The lower O_3 lifetime over remote ocean regions in the warm season combined with the synoptic conditions lead to a decrease of the intercontinental transported O_3 to Europe. Thus, for most receptor regions, the O_3 coming from Asia and rest of the world was reduced by more than half when compared with the cold period. The O_3 concentration from the stratosphere is, in general, 2.5 times higher in the cold season than in the warm season which is consistent witth Butler et al. (2018) study which showed that the stratospheric O_3 concentration varies with altitude and its lifetime is influenced by season and latitude.

10 The tagging technique also helps to quantify the impact of biogenic and biomass burning emissions of NO_x on tropospheric O_3. The impact of biogenic NO_x emissions to the mean O_3 concentrations spans between 3.3 % in ALP and 5.9 % in TCA in the early season, while during the late season it spans between 5.6 % in ALP and 13.4 % in RBU. The biomass burning emissions explain a range of mean O_3 concentration between 1.6 % in ITA to 5.3 % in RBU during early season, and between 3.9 % in ALP and 16.3 % in RBU during late season. Most of the time, the natural sources do not vary greatly when different 15 non-cumulative metrics are applied except for biomass burning emissions on RBU during the late season. Thus, BMB in RBU contributes 16.3 %, 17.6 % and 28.8 % to mean, MDA8 and 95th percentile .

    Even though the SOMO35 and AOT40 metrics are not accumulated over the same time period (SOMO35 – over the entire simulated period, and AOT40 - over the May-July period) and they do not use same input data (daily MDA8 O_3 for SOMO35 vs daytime O_3 concentration for AOT40), since they are based on threshold exceedances and are designed to measure the 20 exposure to high O_3 levels of humans (SOMO35) or vegetation (AOT40), they give us the possibility to directly compare them. As can be seen in Fig. 7 and Table S2, the contribution of different emissions sources and types to the total SOMO35 and AOT40 metrics is similar for most of the European receptor regions. Their spatial distribution (not shown) is also comparable, with minimum values over the UK, NW Europe and Scandinavia and maximum values over Italy, the Alps, south of Spain, east of Turkey and in the metropolitan area of Moscow, Russia, consistent with the previous studies of Aksoyoglu et al. (2014), and 25 Anav et al. (2016). The overseas sources have a similar contribution to the SOMO35 and AOT40 indexes (usually less than 30 %) for most of the receptor regions used in this study. However, in UKI, the overseas sources have a contribution of 32 % to AOT40 and 38 % to SOMO35, and in SCA they have a contribution of ~22 % to AOT40 and 30 % to SOMO35, suggesting that these metrics are sensitive to the O_3 concentration from remote sources in areas having a low level of O_3 pollution. In the RBU receptor region, these indicators are sensitive to O_3 coming from biomass burning emissions (20 % for SOMO35 and 24 % 30 for AOT40), whereas for the remaining receptor regions the contribution of natural sources to SOMO35 and AOT40 is similar. The local sources contribute within a range of ~12 % (SCA)- ~38 % (GEN) to these metrics, accentuating the increased O_3 production from local sources in comparison with northern European countries as well as large emissions of NO_x in the GEN source region. Since the difference in AOT40 and SOMO35 is only a few percent, regardless the receptor region, we could conclude that they are efficiently complementing each other mostly due to the use of a threshold to define these metrics.

The tagging method allows a better understanding of the main precursor sources responsible for exceedances of regulatory O$_3$ metrics. This information can help to inform further modelling studies investigating the effects of emission reduction strategies, and ultimately inform air quality policy. For example, in the ALP region, which includes the Po Valley, the modelled AOT40 is up to 2.6 times higher than the target limit given by EU legislation (on average 23560.8 $\mathrm{ppb-hours}$). The observed and calculated AOT40 values depicted in Figure S3 clearly exhibit the exceedance of target limits in ALP. The O$_3$ coming from local sources explain 33.6 % of this value (AOT40 up to 9163 $\mathrm{ppb-hours}$). After the local sources, the main European anthropogenic sources contributing to high level of AOT40 in the ALP region are distinguished to be FRA (6.5 %), GEN (7.6 %) and MBS (7.9 %) (Table S2). Generally, the O$_3$ concentration and its precursors transported from other anthropogenic European sources to the ALP receptor regions explains ~39 %, the natural sources ~13 % and long range transport ~15 % of the remaining AOT40 concentrations. Thus, to reach at least the target limit in the ALP region, considerable emission reductions are still needed, not only on a local scale, but also on the European scale, especially in the MBS, GER and FRA source region.

Figure 7 also shows the percent contribution of different emissions regions and types to the W126 index. Interestingly, for most of the receptor regions, the local NO$_x$ anthropogenic emissions cause the largest response in W126 compared with the other cumulative metrics used here in this study. Thus, the local NO$_x$ precursors explain from 10.9 % (0.1 $\mathrm{ppm-hours}$) in SCA to more than 40 % of W126 in GEN (45.9 % (2.48 $\mathrm{ppm-hours}$), and ALP (43.5 % (7 $\mathrm{ppm-hours}$)) of W126. The effect of European transported plumes is also enhanced for the W126 index compared with the other metrics for most of the downwind receptor regions. This behaviour is related to the way in which this metrics has been defined. Due to its sigmoidal weighted formulation, as discussed in Westenbarger and Frisvold (1995), and Lapina et al. (2014), W126 takes into account all daytime values; therefore lower weighting factors less than 0.5 are given to low O$_3$ values and weighting factors above 0.5 are given to O$_3$ values situated above the inflection point of 67 ppb. Given that all daytime values are considered by W126 and they are not disregarded as done with SOMO35 and AOT40, we explain why W126 is more sensitive to local NO$_x$ precursors than other metrics.

The modeled mean AOT40 and W126 in the ALP receptor region are exceeding the standards (23560 $\mathrm{ppb-hours}$ for AOT40 and 24.5 $\mathrm{ppm-hours}$ for W126 during the May-July 2010 period) and as we have seen from Fig. 7 and Table S2, the local sources are an important contributor to these metrics. To better understand why the W126 index is mainly influenced by local sources compared with the other cumulative metrics, a more thorough comparison between AOT40 and W126 over the ALP receptor region is presented in the following. Figure 8 presents the temporal series of hourly daylight values for mean O$_3$, W126 and AOT40 averaged over the ALP receptor region. Given that the W126 unit is $\mathrm{ppm-hours}$, for a more direct comparison, the W126 index is expressed in $\mathrm{ppb-hours}$. It can be noted that all metrics have a similar temporal variation, peaking in the first half of July. Also, whenever the averaged O$_3$ concentration is lower than 60 ppb (Fig. 8a), W126 is lower than AOT40 (Fig. 8d), most probably due to the weighting factor less than 0.3, and above this concentration W126 tends to be higher than AOT40. This behavior is closely linked to the definition of these metrics. If the O$_3$ concentration is less than 40 ppb, W126 has a weighting factor lower than 0.03, while AOT40 has a weighting factor of 0. Above this threshold AOT40 has a weighting factor of 1, while in the case of W126 only O$_3$ values higher than 100 ppb have a weighting factor of 1. Due to the

metrics definition, predicted O_3 values in each grid cell are accounted for the W126, and may not be accounted for the AOT40 index.

In addition, the visual analysis of the time series also revealed that when the O_3 concentrations from local sources are ~20 ppb, these concentrations have a higher contribution to W126 than to AOT40. To better understand this, we have further

5   analyzed the relationship between mean O_3 from ALP sources (O_3-ALP) and percent contribution of these O_3 tracers to mean O_3, W126, and AOT40. Figure 9 presents the scatter plots of O_3-ALP and the contribution of these concentrations to mean O_3, W126, and AOT40. In addition, the linear regression of Y vs X (Y=a*X+b) using all data sets has been applied. It can be seen that, in general, high mean O_3-ALP concentrations contributes more to W126 than to AOT40; this is also confirmed by the highest slope (1.64) attained when the linear regression is applied to W126 vs. O_3-ALP. The averaged O_3-ALP and mean O_3

10   as well as O_3-ALP and W126 are highly correlated (r=0.97, and respectively r=0.93), whilst O_3-ALP and AOT40 have a lower correlation (0.88). The high correlation of O_3-ALP with mean O_3 and W126 could be related to the fact that these metrics account for all modeled values, whilst AOT40 considers only O_3 values above 40 ppb.

Extending this analysis to all receptor regions, we can explain why the W126 index is more sensitive to O_3 coming from local sources compared with the other cumulative metrics. In addition, W126 accentuates the contribution of BIO and BMB in RBU,

15   TCA and SEE, most likely because this metric considers all daytime values, and not only those above a certain threshold. Thus, the use of W126 highlights the considerable impact of BIO and BMB emissions which are important sources of O_3 during rhe summer seasons and vegetation fires that ultimately influence the O_3 damage on vegetation.

We have seen that the contribution of different NO_x precursors to total O_3 varies with metrics and with the region. Hence, the tagging method could help design different emission control strategies in specific source regions depending on which impacts

20   need to be reduced in specific receptor
regions.

4   Conclusions

Here, we implemented into the WRF-Chem model a new chemical mechanism to account for source attribution of O_3 from NO_x precursors. We investigated the origin of surface O_3 using the "tagging" technique during April-September 2010 as well

25   as the contribution of different sources to O_3 metrics, and their exceedance events.

Using tagged simulation from WRF-Chem, we show that the spatial distributions of simulated monthly mean MDA8 from tagged O_3 sources regions and types for late spring, summer and early autumn 2010. The contribution of different sources to O_3 production varies with season. We have identified the intercontinental transported O_3 as an important contributor to the total O_3 concentration, especially in the late spring, and early autumn, while during summer the O_3 production is dominated

30   by national and intra-European sources. We have also identified shipping activities in the Mediterranean Sea as an important source of O_3 for the IBE, ITA, SEE, ALP and FRA peripheral maritime receptor regions. We also analysed which are the main sources of MDA8 O_3 over the Mediterranean Basin and our study has identified the main contributors to high MDA8 O_3 concentration, mainly shipping activities and localized contribution from the bordering countries.

To have a better understanding of the origin of MDA8 O_3 exceedances, we compared modelled and observed values of MDA8 O_3 concentration in the Alps and Germany and Benelux receptor regions. Thus, we have seen that during the exceedances days, the contribution from local sources sources is ~45 % and 38 % of modeled MDA8 O_3, whilst during non-exceedances values is ~32 % and 2 3% for ALP, respectively GEN. Moreover, this tagging approach revealed that the main remote sources of MDA8 O_3 are MBS, GEN and FRA for the Alps receptor region, and FRA, CEN and UKI for the Germany and Benelux receptor regions. In addition, this identified a persistently high contribution of transboundary sources to the background O_3 concentration in the ALP region. Furthermore, by showing that the contribution of precursor sources to modelled O_3 target value exceedances in the GEN region is systematically different to the contribution of precursor sources to modelled O_3 when exceedances are observed but not modelled, we have identified a possible reason (underestimation of long-range transport) for the poor performance of our model at reproducing the observed number of O_3 target value exceedances in the GEN region.

By means of different O_3 metrics we quantified the impact of local vs. non local NO_x precursors on O_3 production for each European receptor region. The comparison between mean, MDA8 and 95th percentile O_3 metrics accentuate the importance of large contributions from different NO_x precursors to the high-end of the O_3 distribution. By analysing these metrics for two periods (April-June and July-September), we can clearly distinguish the contribution of different NO_x precursors to total O_3 concentration in each region for different times of the year. When we compare the cumulative metrics, we notice that the SOMO35 and AOT40 indexes exhibit a rather similar behaviour. Considering that these metrics are not calculated over the same time period nor do they use same input data, the similar behaviour is likely due to the similar threshold values applied to define these metrics.

The use of the W126 index accentuates the importance of local emissions. To confirm this, we investigated the behaviour of modeled mean AOT40 and W126 in the ALP receptor region. We noticed that when the O_3 concentrations from local sources are approximately 20 ppb, these concentrations have a higher contribution to W126 than to AOT40, mostly due to the definition of W126 which takes into account all O_3 values, not only those that are above a certain threshold.

Overall, this study has identified the local and remote contribution to the MDA8 O_3 concentration during several periods as well as to different O_3 metrics. Furthermore, the method applied here could be used to design different emission control strategies depending on which impacts need to be reduced.

Appendix A

– chemics_init.F;

– module_input_chem_data.F;

– module_plumerise1.F and module_add_emiss_burn.F to account the source attribution of biomass burning emissions to O_3 concentration;

– module_emissions_anthropogenics.F to account for the impact of anthropogenic emissions on O_3 concentration;

- module_bioemi_megan2.F and module_data_mgn2mech.F to see the impact of biogenic emissions on O_3 concentration;

- module_lightning_nox_driver.F for lightning-generated nitrogen oxides

- Dry and wet deposition of tagged trace gases are treated by module_dep_simple.F and module_mozcart_wetscav.F, thus all tagged species have the same dry deposition velocities and wet removal rates with the corresponding non-tagged species;

- module_ftuv_driver.F to consider the photolytical reaction of the new packages;

- emissions_driver.F;

- chem_driver.F.

Code and data availability. The WRF-Chem model is publicly available on http://www2. mmm.ucar.edu/wrf/users/download/get_source.html. The modification introduced and described in Section 2 as well as the model data can be provided upon request to the corresponding author.

Author contributions. AL and TB designed the research. AL adapted the automatic mechanism-rewriting and code-generation tools and in implemented into WRF-Chem source code. AL performed the model runs and subsequent analysis. AL wrote the pape with contribution from TB.

Acknowledgements. This work was hosted by IASS Potsdam, with financial support provided by the Federal Ministry of Education and Research of Germany (fBMBF) and the Ministry for Science, Research and Culture of the State of Brandenburg (MWFK). The authors would like to thank Kathleen Mar for helping with the emissions preprocessing as well as to Jane Coates for her help with some of the plots.

References

Agathokleous, E., Kitao, M., and Kinose, Y. .: A Review Study on Ozone Phytotoxicity Metrics for Setting Critical Levels in Asia, Asian Journal of Atmospheric Environment, 12, 1–16, https://doi.org/https://doi.org/10.5572/ajae.2018.12.1.001, 2018.

Aksoyoglu, S., Keller, J., Ciarelli, G., Prévôt, A. S. H., and Baltensperger, U.: A model study on changes of European and Swiss particulate

5 matter, ozone and nitrogen deposition between 1990 and 2020 due to the revised Gothenburg protocol, Atmos. Chem. Phys., 14, 13 081–13 095, https://doi.org/https://doi.org/10.5194/acp-14-13081-2014, 2014.

Aksoyoglu, S., Baltensperger, U., and Prévôt, A. S. H.: Contribution of ship emissions to the concentration and deposition of air pollutants in Europe, Atmos. Chem. Phys., 16, 1895–1906, https://doi.org/https://doi.org/10.5194/acp-16-1895-2016, 2016.

Anav, A., De Marco, A., Proietti, C., Alessandri, A., Dell'Aquila, A., Cionni, I., Friedlingstein, P., Khvorostyanov, D., Menut, L., Pao-

10 letti, E., Sicard, P., Sitch, S., Vitale, M., Anav, A., De Marco, A., and Proietti, C.: Comparing concentration-based (AOT40) and stomatal uptake (PODY) metrics for ozone risk assessment to European forests, Global Change Biology (2016), 22, 1608–1627, https://doi.org/10.1111/gcb.13138, 2016.

Avnery, S., Mauzerall, D. L., L, D., and Fiore, A. M.: Increasing global agricultural production by reducing ozone damages via methane emission controls and ozone-resistant cultivar selection, Glob. Change Biol., 19, 1285–1299, https://doi.org/10.1111/Gcb.12118, 2013.

15 Butler, T., Lupascu, A., Coates, J. a., and Zhu, S.: TOAST 1.0: Tropospheric Ozone Attribution of Sources with Tagging for CESM 1.2.2, Geosci. Model Dev., 11, 2825–2840, https://doi.org/https://doi.org/10.5194/gmd-11-2825-2018, 2018.

Chan, C. K. and Yao, X.: Air pollution in mega cities in China, Atmos. Environ., 42, 1–42, https://doi.org/10.1016/j.atmosenv.2007.09.003, 2008.

Chou, M.-D. and Suarez, M. J.: An efficient thermal infrared radiation parametrization for use in general circulation models, NASA Tech.

20 Memo., 104606, 85 pp, 1994.

Christensen, J. H. and Christensen, O. B.: A summary of the PRUDENCE model projections of changes in European climate by the end of this century, Climatic Change, 81(Suppl 1): 7, https://doi.org/doi:10. 1007/s10584-006-9210-7, 2007.

Colette, A., Granier, C., Hodnebrog, ., Jakobs, H., Maurizi, A., Nyiri, A., Rao, S., Amann, M., Bessagnet, B., D'Angiola, A., Gauss, M., Heyes, C., Klimont, Z., Meleux, F., Memmesheimer, M., Mieville, A., Rouïl, L., Russo, F., Schucht, S., Simpson, D., Stordal, F., Tampieri,

25 F., and Vrac, M.: Future air quality in Europe: a multi-model assessment of projected exposure to ozone, Atmos. Chem. Phys., 12, 10 613–10 630, https://doi.org/10.5194/acp-12-10613-2012, 2012.

Dahlmann, K., Grewe, V., Ponater, M., and Matthes, S.: Quantifying the contributions of individual NOx sources to the trend in ozone radiative forcing, Atmos. Environ., 45, 2860–2868, https://doi.org/10.1016/j.atmosenv.2011.02.071, 2011.

Danielsen, E. F.: Stratospheric-tropospheric exchange based on radioactivity ozone and potential vorticity, J. Atmos. Sci., 2, 502–518,

30 https://doi.org/https://doi.org/10.1175/1520-0469(1968)025<0502:STEBOR>2.0.CO;2, 1968.

Derwent, R. G., Utember, S. R., Jenkin, M. E., and Shallcross, D. E.: Tropospheric ozone production regions and the intercontinental origins of surface ozone over Europe, Atmos. Environ., p. 216–224, 2015.

EEA: AirbAse - The European air quality database, available at: https://www.eea.europa.eu/data-and-maps/data/aqereporting-8, (last access: 12 September 2018), 2017.

35 Emmons, L. K., Hess, P. G., Lamarque, J.-F., and Pfister, G. G.: Tagged ozone mechanism for MOZART-4, CAM-chem and other chemical transport models, Geoscientific Model Development, 5, 1531–1542, https://doi.org/10.5194/gmd-5-1531-2012, https://www.geosci-model-dev.net/5/1531/2012/, 2012.

EU directive 2008/50/EC: EU directive 2008/50/EC of the European parliament and of the council on Ambient Air Quality and Cleaner Air for Europe (http://eur-lex.europa.eu/LexUriServ/LexUriServ.do?uri=OJ:L:2008:152:0001:0044:en:PDFm, last accessed April 6, 2018), 2008.

European Commission: Forest Fires in Europe 2010, Luxembourg: Publications Office of the European Union, EUR 24910 EN, ISBN 978-92-79-20919-2, 2011.

Fiore, A., Dentener, F. J., Wild, O., Cuvelier, C., Schultz, M. G., Hess, P., Textor, C., Schulz, M., Doherty, R. M., Horowitz, L. W., MacKenzie, I. A., Sanderson, M. G., Shindell, D. T., Stevenson, D. S., Szopa, S., Dingenen, R. V., Zeng, G., Atherton, C., Bergmann, D., Bey, I., Carmichael, G., Collins, W. J., Duncan, B. N., Faluvegi, G., Folberth, G., Gauss, M., Gong, S., Hauglustaine, D., Holloway, T., Isaksen, I. S. A., Jacob, D. J., Jonson, J. E., Kaminski, J. W., Keating, T. J., Lupu, A., Marmer, E., Montanaro, V., Park, R. J., Pitari, G., Pringle, K. J., Pyle, J. A., Schroeder, S., Vivanco, M. G., Wind, P., Wojcik, G., Wu, S., and Zuber, A.: Multimodel estimates of intercontinental source-receptor relationships for ozone pollution, Journal of Geophysical Research: Atmospheres, 114, https://doi.org/10.1029/2008JD010816, 2009.

Flemming, J., Huijnen, V., Arteta, J., Bechtold, P., Beljaars, A., Blechschmidt, A.-M., Diamantakis, M., Engelen, R. J., Gaudel, A., Inness, A., Jones, L., Josse, B., Katragkou, E., Marecal, V., Peuch, V.-H., Richter, A., Schultz, M. G., Stein, O., and Tsikerdekis, A.: Tropospheric chemistry in the Integrated Forecasting System of ECMWF, Geoscientific Model Development, 8, 975–1003, https://doi.org/10.5194/gmd-8-975-2015, https://www.geosci-model-dev.net/8/975/2015/, 2015.

Gao, J., Zhu, B., Xiao, H., Kang, H., Hou, X., and Shao, P.: A case study of surface ozone source apportionment during a high concentration episode, under frequent shifting wind conditions over the Yangtze River Delta, China, Science of the Total Environment, 544, 853–863, https://doi.org/http://dx.doi.org/10.1016/j.scitotenv.2015.12.039, 2016.

Gilbert, N.: Russia counts environmental cost of wildfires, Nature News, https://doi.org/doi:10.1038/news.2010.404, 2010.

Giordano, L., Brunner, D., Flemming, J., Hogrefe, C., Im, U., Bianconi, R., Badia, A., Balzarini, A., Baro, R., Chemel, C., Curci, G., Forkel, R., Jimenez-Guerrero, P., Hirtl, M., Hodzic, A., Honzak, L., Jorba, O., Knote, C., Kuenen, J. J. P., Makar, P. A., Manders-Groot, A., Neal, L., Perez, J. L., Pirovano, G., Pouliot, G., San Jose, R., Savage, N., Schroder, W., Sokhi, R. S., Syrakov, D., Torian, A., Tuccella, P., Werhahn, J., Wolke, R., Yahya, K., Žabkar, R., Zhang, Y., and Galmarini, S.: Assessment of the MACC re-analysis and its influence as chemical boundary conditions for regional air quality modeling in AQMEII-2, Atmos. Environ., 115, 371–388, 2015.

Grell, G. A. and Freitas, S. R.: A scale and aerosol aware stochastic convective parameterization for weather and air quality modeling, Atmospheric Chemistry and Physics, 14, 5233–5250, https://doi.org/10.5194/acp-14-5233-2014, https://www.atmos-chem-phys.net/14/5233/2014/, 2014.

Grell, G. A., Peckham, S. E., Schmitz, R., McKeen, S. A., Frost, G., Skamarock, W. C., and Eder, B.: Fully coupled online chemistry within the WRF model, Atmos. Environ., 39, 6957–6975, 2005.

Grewe, V., Tsati, E., and Hoor, P.: On the attribution of contributions of atmospheric trace gases to emissions in atmospheric model applications, Geoscientific Model Development, 3, 487–499, https://doi.org/10.5194/gmd-3-487-2010, https://www.geosci-model-dev.net/3/487/2010/, 2010.

Grewe, V., Dahlmann, K., Matthes, S., and Steinbrecht, W.: Attributing ozone to NOx emissions: Implications for climate mitigation measures, Atmos. Environ., 59, 102–107, https://doi.org/doi:10.1016/j.atmosenv.2012.05.002:, 2012.

Grewe, V., Tsati, E., Mertens, M., Fromming, C., and Jockel, P.: Contribution of emissions to concentrations: the TAGGING 1.0 submodel based on the Modular Earth Submodel System (MESSy 2.52), Geoscientific Model Development, 10, 2615–2633, https://doi.org/10.5194/gmd-10-2615-2017, https://www.geosci-model-dev.net/10/2615/2017/, 2017.

Gromov, S., Jöckel, P., Sander, R., and Brenninkmeijer, C. A. M.: A kinetic chemistry tagging technique and its application to modelling the stable isotopic composition of atmospheric trace gases, Geoscientific Model Development, 3, 337–364, https://doi.org/10.5194/gmd-3-337-2010, https://www.geosci-model-dev.net/3/337/2010/, 2010.

Guenther, A., Karl, T., Harley, P., Wiedinmyer, C., Palmer, P. I., and Geron, C.: Estimates of global terrestrial isoprene emissions using MEGAN (Model of Emissions of Gases and Aerosols from Nature), Atmospheric Chemistry and Physics, 6, 3181–3210, https://doi.org/10.5194/acp-6-3181-2006, https://www.atmos-chem-phys.net/6/3181/2006/, 2006.

Hong, S.-Y., Noh, Y., and Dudhia, J.: A new vertical diffusion package with an explicit treatment of entrainment processes, Mon. Weather Rev., 134, 2318–2341, https://doi.org/10.1175/MWR3199.1, 2006.

HTAP: HTAP: Hemispheric Transport of Air Pollution 2010, Part A: Ozone and Particulate Matter, Air Pollution Studies,No.17, Geneva, Switzerland, 2010.

Huijnen, V., Flemming, J., Kaiser, J. W., Inness, A., Leitão, J., Heil, A., Eskes, H. J., Schultz, M. G., Benedetti, A., Hadji-Lazaro, J., Dufour, G., and Eremenko, M.: Hindcast experiments of tropospheric composition during the summer 2010 fires over western Russia, Atmospheric Chemistry and Physics, 12, https://doi.org/10.5194/acp-12-4341-2012, https://www.atmos-chem-phys.net/12/4341/2012/, 2012.

Iacono, M., Delamere, J., Mlawer, E., Shephard, M., Clough, S., and Collins, W.: Radiative forcing by long-lived greenhouse gases: Calculations with the AER radiative transfer models, J. Geophys. Res.-Atmos., 113, https://doi.org/10.1029/2008JD009944, 2008.

Im, U., Christensen, J. H., Geels, C., Hansen, K. M., Brandt, J., Solazzo, E., Alyuz, U., Balzarini, A., Baro, R., Bellasio, R., Bianconi, R., Bieser, J., Colette, A., Curci, G., Farrow, A., Flemming, J., Fraser, A., Jimenez-Guerrero, P., Kitwiroon, N., Liu, P., Nopmongcol, U., Palacios-Peña, L., Pirovano, G., Pozzoli, L., Prank, M., Rose, R., Sokhi, R., Tuccella, P., Unal, A., Vivanco, M. G., Yarwood, G., Hogrefe, C., and Galmarini, S.: Influence of anthropogenic emissions and boundary conditions on multi-model simulations of major air pollutants over Europe and North America in the framework of AQMEII3, Atmospheric Chemistry and Physics, 18, 8929–8952, https://doi.org/10.5194/acp-18-8929-2018, https://www.atmos-chem-phys.net/18/8929/2018/, 2018.

Jimenez, P. A. and Dudhia, J.: Improving the Representation of Resolved and Unresolved Topographic Effects on Surface Wind in the WRF Model, J. Appl Meteor. and Climo, 51, 300–316, https://doi.org/https://doi.org/10.1175/JAMC-D-11-084.1, 2012.

Jiménez, P., Lelieveld, J., and Baldasano, J. M.: Multiscale modeling of air pollutants dynamics in the northwestern Mediterranean basin during a typical summertime episode, Journal of Geophysical Research: Atmospheres, 111, https://doi.org/10.1029/2005JD006516, 2006.

Jiménez, P., Dudhia, J., González-Rouco, J., Navarro, J., Montávez, J., and García-Bustamante, E.: A revised scheme for the WRF surface layer formulation, Mon. Weather Rev., 140, 898–918, https://doi.org/10.1175/MWR-D-11-00056.1, 2012.

Kuenen, J. J. P., Visschedijk, A. J. H., Jozwicka, M., and Denier van der Gon, H. A. C.: TNO-MACCII emission inventory; a multi-year (2003-2009) consistent high-resolution European emission inventory for air quality modelling, Atmospheric Chemistry and Physics, 14, 10 963–10 976, https://doi.org/10.5194/acp-14-10963-2014, https://www.atmos-chem-phys.net/14/10963/2014/, 2014.

Lapina, K., Henze, D. K., Milford, J. B., Huang, M., Lin, M., Fiore, A. M., Carmichael, G., Pfister, G. G., and Bowman, K.: Assessment of source contributions to seasonal vegetative exposure to ozone in the U.S., Journal of Geophysical Research: Atmospheres, 119, 324–340, https://doi.org/10.1002/2013JD020905, 2014.

Lefohn, A., Malley, C., Smith, L., Wells, B., Hazucha, M., Simon, H., Naik, V., Mills, G., Schultz, M., Paoletti, E., De Marco, A., Xu, X., Zhang, L., Wang, T., Neufeld, H., Musselman, R., Tarasick, D., Brauer, M., Feng, Z., Tang, H., Kobayashi, K., Sicard, P., Solberg, S., and Gerosa, G.: Tropospheric ozone assessment report: Global ozone metrics for climate change, human health, and crop/ecosystem research, Elem Sci Anth, 6(1), 28, https://doi.org/https://doi.org/10.1525/elementa.279, 2018.

Lefohn, A. S., Laurence, J. A., and Kohut, R. J.: A comparison of indices that describe the relationship between exposure to ozone and reduction in the yield of agricultural crops, Atmospheric Environment (1967), 22, 1229 – 1240, https://doi.org/https://doi.org/10.1016/0004-6981(88)90353-8, 1988.

Li, G., Zhang, R., Fan, J., and Tie, X.: Impacts of black carbon aerosol on photolysis and ozone, Journal of Geophysical Research: Atmospheres, 110, https://doi.org/10.1029/2005JD005898, 2005.

Li, J., Yang, W., Wang, Z., Chen, H., Hu, B., Li, J., Sun, Y., Fu, P., and Zhang, Y.: Modeling study of surface ozone source-receptor relationships in East Asia, Atmospheric Research, 167, 77 – 88, https://doi.org/https://doi.org/10.1016/j.atmosres.2015.07.010, 2016.

Mar, K., Ojha, N., Pozzer, A., and Butler, T.: Ozone air quality simulations with WRF-Chem (v3.5.1) over Europe: Model evaluation and chemical mechanism comparison, Geosci. Model Dev., 9, 3699–3728, https://doi.org/10.5194/gmd-9-3699-2016, 2016.

Mertens, M., Grewe, V., Rieger, V. S., and Jöckel, P.: Revisiting the contribution of land transport and shipping emissions to tropospheric ozone, Atmospheric Chemistry and Physics, 18, 5567–5588, https://doi.org/10.5194/acp-18-5567-2018, https://www.atmos-chem-phys.net/18/5567/2018/, 2018.

Morrison, H., Thompson, G., and Tatarskii, V.: Impact of cloud microphysics on the development of trailing stratiform precipitation in a simulated squall line: Comparison of one- and two-moment schemes, Monthly Weather Review, 137, 991–1007, https://doi.org/10.1175/2008MWR2556.1, 2009.

Musselman, R., Lefohn, A., Massman, W., and Heath, R.: A critical review and analysis of the use of exposure- and flux-based ozone indices for predicting vegetation effects, Atmospheric Environment, 40, 1869–1888, https://doi.org/10.1016/j.atmosenv.2005.10.064, 2006.

Neu, J. L. and Prather, M. J.: Toward a more physical representation of precipitation scavenging in global chemistry models: cloud overlap and ice physics and their impact on tropospheric ozone, Atmospheric Chemistry and Physics, 12, 3289–3310, https://doi.org/10.5194/acp-12-3289-2012, https://www.atmos-chem-phys.net/12/3289/2012/, 2012.

Otero, N., Sillmann, J., Mar, K. A., Rust, H. W., Solberg, S., Andersson, C., Engardt, M., Bergström, R., Bessagnet, B., Colette, A., Couvidat, F., Cuvelier, C., Tsyro, S., Fagerli, H., Schaap, M., Manders, A., Mircea, M., Briganti, G., Cappelletti, A., Adani, M., D'Isidoro, M., Pay, M.-T., Theobald, M., Vivanco, M. G., Wind, P., Ojha, N., Raffort, V., and Butler, T.: A multi-model comparison of meteorological drivers of surface ozone over Europe, Atmospheric Chemistry and Physics, 18, 12 269–12 288, https://doi.org/10.5194/acp-18-12269-2018, https://www.atmos-chem-phys.net/18/12269/2018/, 2018.

Paoletti, E., De Marco, A., and Racalbuto, S.: Why should we calculate complex indices of ozone exposure? Results from Mediterranean background stations, Environmental Monitoring and Assessment, 128, 19–30, https://doi.org/10.1007/s10661-006-9412-5., 2007.

Pfister, G. G., Avise, J., Wiedinmyer, C., Edwards, D. P., Emmons, L. K., Diskin, G. D., Podolske, J., and Wisthaler, A.: CO source contribution analysis for California during ARCTAS-CARB, Atmospheric Chemistry and Physics, 11, 7515–7532, https://doi.org/10.5194/acp-11-7515-2011, https://www.atmos-chem-phys.net/11/7515/2011/, 2011.

Pfister, G. G., Walters, S., Emmons, L. K., Edwards, D. P., and Avise, J.: Quantifying the contribution of inflow on surface ozone over California during summer 2008, Journal of Geophysical Research: Atmospheres, 118, 12,282–12,299, https://doi.org/10.1002/2013JD020336, 2013.

Querol, X., Alastuey, A., Gangoiti, G., Perez, N., Lee, H. K., Eun, H. R., Park, Y., Mantilla, E., Escudero, M., Titos, G., Alonso, L., Temime-Roussel, B., Marchand, N., Moreta, J. R., Revuelta, M. A., Salvador, P., Artíñano, B., García dos Santos, S., Anguas, M., Notario, A., Saiz-Lopez, A., Harrison, R. M., Millán, M., and Ahn, K.-H.: Phenomenology of summer ozone episodes over the Madrid Metropolitan Area, central Spain, Atmospheric Chemistry and Physics, 18, 6511–6533, https://doi.org/10.5194/acp-18-6511-2018, https://www.atmos-chem-phys.net/18/6511/2018/, 2018.

Ramaswamy, V., Boucher, O., Haigh, J., Hauglustaine, D., Haywood, J., Myhre, G., Nakajima, T., Shi, G., and 2001, S. S.: Radiative forcing of climate change, In: Climate Change 2001: The Scientific Basis,Contribution of WG1 to the Third Assessment Report of the IPCC, Houghton, J.T. et al. (eds), Cambridge University Press, England, 2001.

Safieddine, S., Boynard, A., Coheur, P.-F., Hurtmans, D., Pfister, G., Quennehen, B., Thomas, J. L., Raut, J.-C., Law, K. S., Klimont, Z., Hadji-Lazaro, J., George, M., and Clerbaux, C.: Summertime tropospheric ozone assessment over the Mediterranean region using the thermal infrared IASI/MetOp sounder and the WRF-Chem model, Atmospheric Chemistry and Physics, 14, 10 119–10 131, https://doi.org/10.5194/acp-14-10119-2014, https://www.atmos-chem-phys.net/14/10119/2014/, 2014.

Sandu, A. and Sander, R.: Technical note: Simulating chemical systems in Fortran90 and Matlab with the Kinetic PreProcessor KPP-2.1, Atmospheric Chemistry and Physics, 6, 187–195, https://doi.org/10.5194/acp-6-187-2006, https://www.atmos-chem-phys.net/6/187/2006/, 2006.

Stevenson, D. S., Young, P. J., Naik, V., Lamarque, J.-F., Shindell, D. T., Voulgarakis, A., Skeie, R. B., Dalsoren, S. B., Myhre, G., Berntsen, T. K., Folberth, G. A., Rumbold, S. T., Collins, W. J., MacKenzie, I. A., Doherty, R. M., Zeng, G., van Noije, T. P. C., Strunk, A., Bergmann, D., Cameron-Smith, P., Plummer, D. A., Strode, S. A., Horowitz, L., Lee, Y. H., Szopa, S., Sudo, K., Nagashima, T., Josse, B., Cionni, I., Righi, M., Eyring, V., Conley, A., Bowman, K. W., Wild, O., and Archibald, A.: Tropospheric ozone changes, radiative forcing and attribution to emissions in the Atmospheric Chemistry and Climate Model Intercomparison Project (ACCMIP), Atmospheric Chemistry and Physics, 13, 3063–3085, https://doi.org/10.5194/acp-13-3063-2013, https://www.atmos-chem-phys.net/13/3063/2013/, 2013.

Struzewska, J., Zdunek, M., Kaminski, J. W., Łobocki, L., Porebska, M., Jefimow, M., and Gawuc, L.: Evaluation of the GEM-AQ model in the context of the AQMEII Phase 1 project, Atmospheric Chemistry and Physics, 15, 3971–3990, https://doi.org/10.5194/acp-15-3971-2015, https://www.atmos-chem-phys.net/15/3971/2015/, 2015.

Sudo, K. and Akimoto, H.: Global source attribution of tropospheric ozone: Long-range transport from various source regions, Journal of Geophysical Research Atmospheres, 112, https://doi.org/10.1029/2006JD007992, 2007.

Tagaris, E., Stergiou, I., and Sotiropoulou, R.: Impact of shipping emissions on ozone levels over Europe: assessing the relative importance of the Standard Nomenclature for Air Pollution (SNAP) categories, Environmental Science and Pollution Research, 24, 14 903–14 909, https://doi.org/0.1007/s11356-017-9046-x, https://doi.org/10.1007/s11356-017-9046-x, 2017.

Tai, A. P. and Val Martin, M.: Impacts of ozone air pollution and temperature extremes on crop yields: Spatial variability, adaptation and implications for future food security, Atmospheric Environment, 169, 11 – 21, https://doi.org/https://doi.org/10.1016/j.atmosenv.2017.09.002, 2017.

Tang, Y., Carmichael, G., Thongboonchoo, N., Chai, T., Horowitz, L., Pierce, R., Al-Saadi, J., Pfister, G., Vukovich, J., Avery, M., Sachse, G., Ryerson, T., Holloway, J., Atlas, E., Flocke, F., Weber, R., Huey, L., Dibb, J., Streets, D., and Brune, W.: Influence of lateral and top boundary conditions on regional air quality prediction: A multiscale study coupling regional and global chemical transport models, Journal of Geophysical Research Atmospheres, 112, https://doi.org/10.1029/2006JD007515, 2007.

Thouret, V., Cammas, J.-P., Sauvage, B., Athier, G., Zbinden, R., Nédélec, P., Simon, P., and Karcher, F.: Tropopause referenced ozone climatology and inter-annual variability (1994–2003) from the MOZAIC programme, Atmospheric Chemistry and Physics, 6, 1033–1051, https://doi.org/10.5194/acp-6-1033-2006, https://www.atmos-chem-phys.net/6/1033/2006/, 2006.

Tie, X., Madronich, S., Walters, S., Zhang, R., Rasch, P., and Collins, W.: Effect of clouds on photolysis and oxidants in the troposphere, Journal of Geophysical Research: Atmospheres, 108, https://doi.org/10.1029/2003JD003659, 2003.

Tong, D., Mathur, R., Kang, D., Yu, S., Schere, K., and Pouliot, G.: Vegetation exposure to ozone over the continental United States: Assessment of exposure indices by the Eta-CMAQ air quality forecast model, Atmospheric Environment, 43, 724–733, https://doi.org/10.1016/j.atmosenv.2008.09.084, 2009.

Tuccella, P., Curci, G., Visconti, G., Bessagnet, B., Menut, L., and Park, R.: Modeling of gas and aerosol with WRF/Chem over Europe:

5 Evaluation and sensitivity study, Journal of Geophysical Research Atmospheres, 117, https://doi.org/10.1029/2011JD016302, 2012.

UNECE: Mapping Critical Levels for Vegetation. International Cooperative Programme on Effects of Air Pollution on Natural Vegetation and Crops, Bangor, UK, 2010.

Vijayaraghavan, K., Cho, S., Morris, R., Spink, D., Jung, J., Pauls, R., and Duffett, K.: Photochemical model evaluation of the ground-level ozone impacts on ambient air quality and vegetation health in the Alberta oil sands region: Using present and future emission scenarios,

10 Atmospheric Environment, 141, 209–218, https://doi.org/10.1016/j.atmosenv.2016.06.053, 2016.

Wang, Z., Chien, C.-J., and Tonnesen, G.: Development of a tagged species source apportionment algorithm to characterize three-dimensional transport and transformation of precursors and secondary pollutants, Journal of Geophysical Research Atmospheres, 114, https://doi.org/10.1029/2008JDO10846, 2009.

Wesely, M.: Parameterization of surface resistances to gaseous dry deposition in regional-scale numerical models, Atmospheric Environment

15 (1967), 23, 1293–1304, https://doi.org/10.1016/0004-6981(89)90153-4, 1989.

Westenbarger, D. A. and Frisvold, G.: Air pollution and farm level crop yields: an empirical analysis of corn and soybeans, Agric. Resour. Econ. Rev., 24 (1995), 156–165, 1995.

WHO: Quantification of health effects of exposure to air pollution, EUR/01/5026342, E74256, WHO Regional office for Europe, Copenhagen, Available at: http://www.euro.who.int/document/e74256.pdf (last accessed 20 April 2018), 2001.

20 WHO: Air quality guidelines. Global update 2005. Particulate matter, ozone, nitrogen dioxide and sulfur dioxide, World Health Organizations 2006, pp. ix+484 pages, ISBN 9289021 926, https://doi.org/http://www.euro.who.int/__data/assets/pdf_file/0005/78638/E90038.pdf?ua=1 (last accessed, 18 April 2016), 2006.

WHO: Evolution of WHO air quality guidelines: past, present and future, World Health Organizations, (last accessed 1 August 2017), pp. vi+32 pages, https://doi.org/ISBN9789289052306, 2017.

25 Wiedinmyer, C., Akagi, S. K., Yokelson, R. J., Emmons, L. K., Al-Saadi, J. A., Orlando, J. J., and Soja, A. J.: The Fire INventory from NCAR (FINN): a high resolution global model to estimate the emissions from open burning, Geoscientific Model Development, 4, 625–641, https://doi.org/10.5194/gmd-4-625-2011, https://www.geosci-model-dev.net/4/625/2011/, 2011.

Yarwood, G., Morris, R., Yocke, M., Hogo, H., and Chico, T.: Development of a Methodology for Source Apportionment of Ozone Concentrations Estimates From a Photo-chemical Grid Model, Air and Waste management association, p. 15222, 1996.

Table 1. List of tagged European source/receptor regions

Acronym	List of countries
MBS	Mediterranean, and Black Seas
BNS	Baltic, and North Seas
CEN	East Austria, Hungary, Czech Republic, Slovakia, Estonia, Latvia, Lithuania, Poland
ALP	West Austria, Switzerland, and North Italy (including Po Valley)
ITA	South Italy, and Malta
SEE	Bulgaria, Romania, Moldavia, Albania, Slovenia, Croatia, Serbia, Montenegro, Macedonia, Greece, and Cyprus
IBE	Spain, and Portugal
UKI	United Kingdom, and Ireland
GEN	Belgium, Netherland, Luxembourg, and Germany
SCA	Finland, Norway, Sweden, Denmark, and Island
FRA	France
RBU	Russia, Belarus, and Ukraine
TCA	Turkey, Azerbaijan, Armenia, and Georgia

Table 2. Observed mean and simulation summary statistics for meteorological parameters. The normalized mean bias (NMB) and correlation coefficient (R) are calculated between simulated and observed meteorological observation from GWO during April – September 2010 period

Variable	Observed			Modeled mean			NMB (%)	R
	min	mean	max	min	mean	max		
MSLP	1000.96	1014.3	1022.06	969.05	1014.5	1039.03	-0	0.98
T2M	-17.14	14.99	32.10	-22.50	14.76	43.45	-3	0.91
WS10M	0.36	3.37	10.83	0.00	3.59	20.41	8	0.65
WD10M	0	190	360	31.91	216	318	13	0.47

Table 3. Observed mean and simulation summary statistics for MDA8 O_3 concentrations ($\mu g/m^{-3}$) at rural background sites. The normalized mean bias (NMB) and correlation coefficient (R) are calculated between simulated and observed O_3 concentrations from the AirBase dataset during April – September 2010 period.

Analyzed period	Observed			Modeled			NMB (%)	R
	min	mean	max	min	mean	max		
April	52.5	97.0	140.8	36.5	90.8	134.5	-6.3	0.58
May	41.0	87.9	143.0	28.0	83.2	124.6	-5.4	0.62
June	44.2	96.2	162.3	32.0	89.7	132.6	-6.8	0.71
July	43.8	97.0	178.2	26.0	90.8	147.7	-6.3	0.58
August	40.3	87.5	145.2	27.3	82.6	130.8	-5.6	0.65
September	33.4	77.5	135.4	26.5	81.1	129.6	4.6	0.63
Total	40.5	90.5	160.5	28.4	86.3	135.9	-5.2	0.69
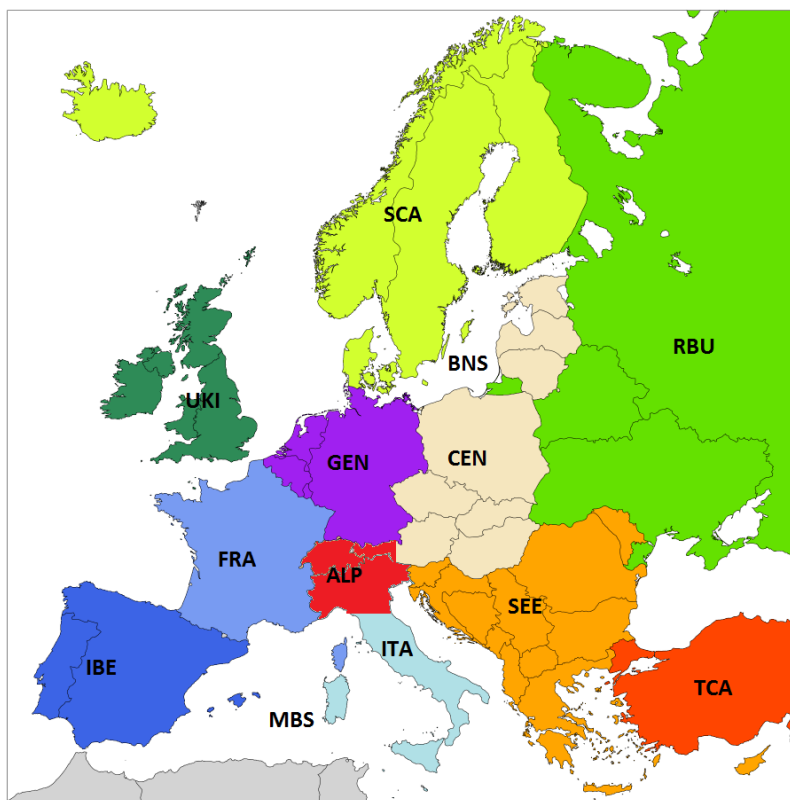
Figure 1. Tagged European source/receptor regions
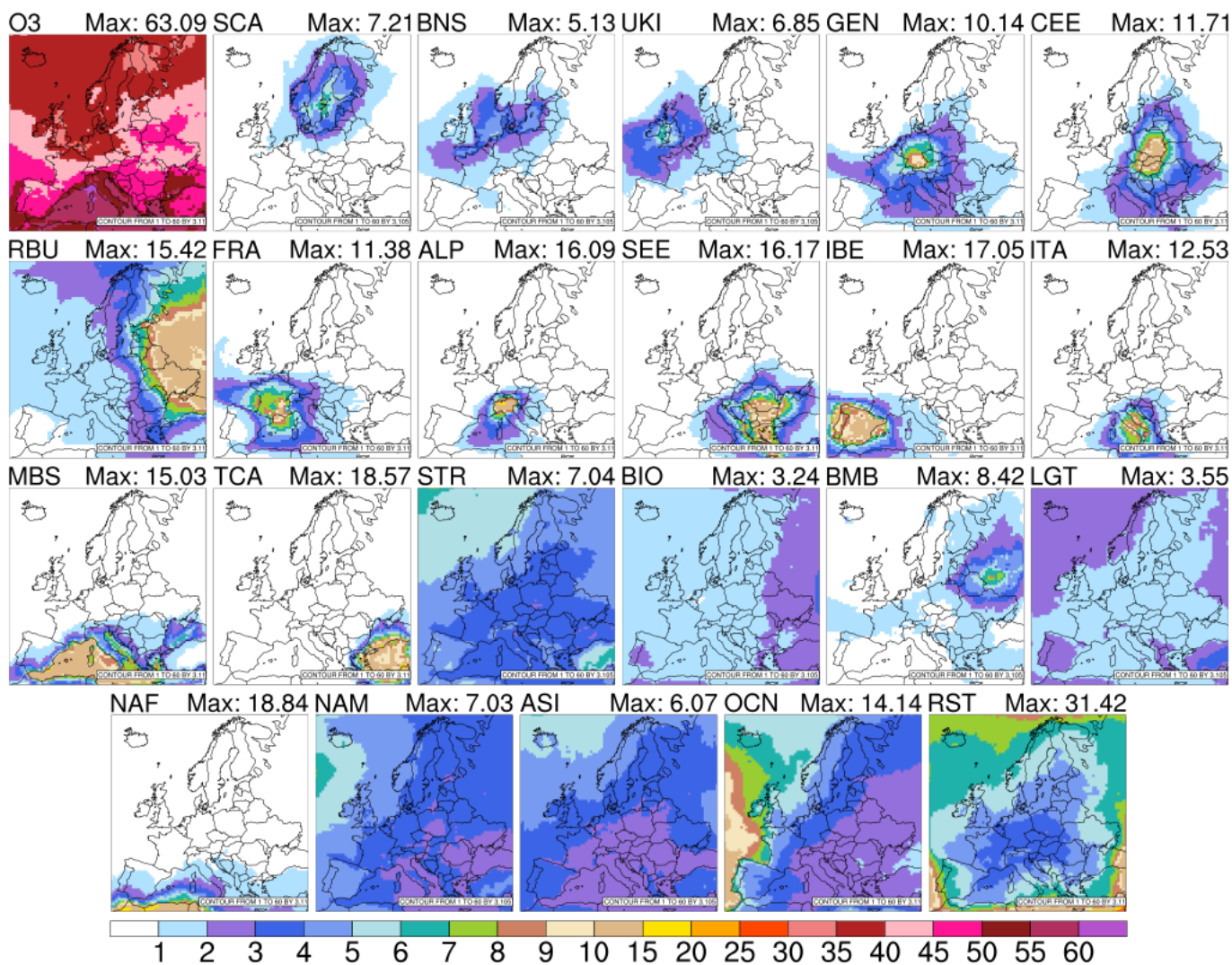
Figure 2. Contribution to MDA8 O$_3$ (ppb) of each O$_3$ source region for the April-May 2010 period
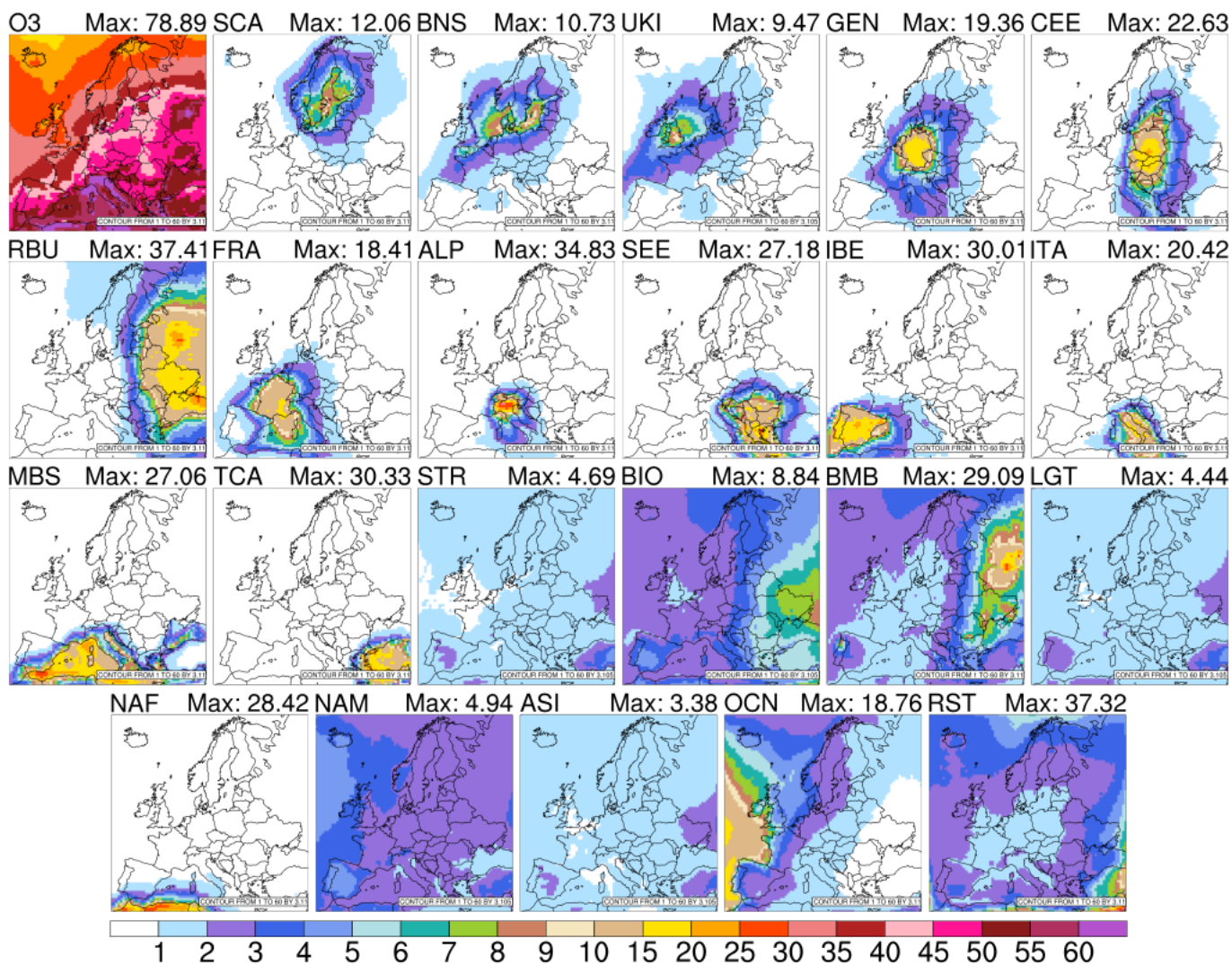
Figure 3. Same as Fig. 2, but for the June-August 2010 period
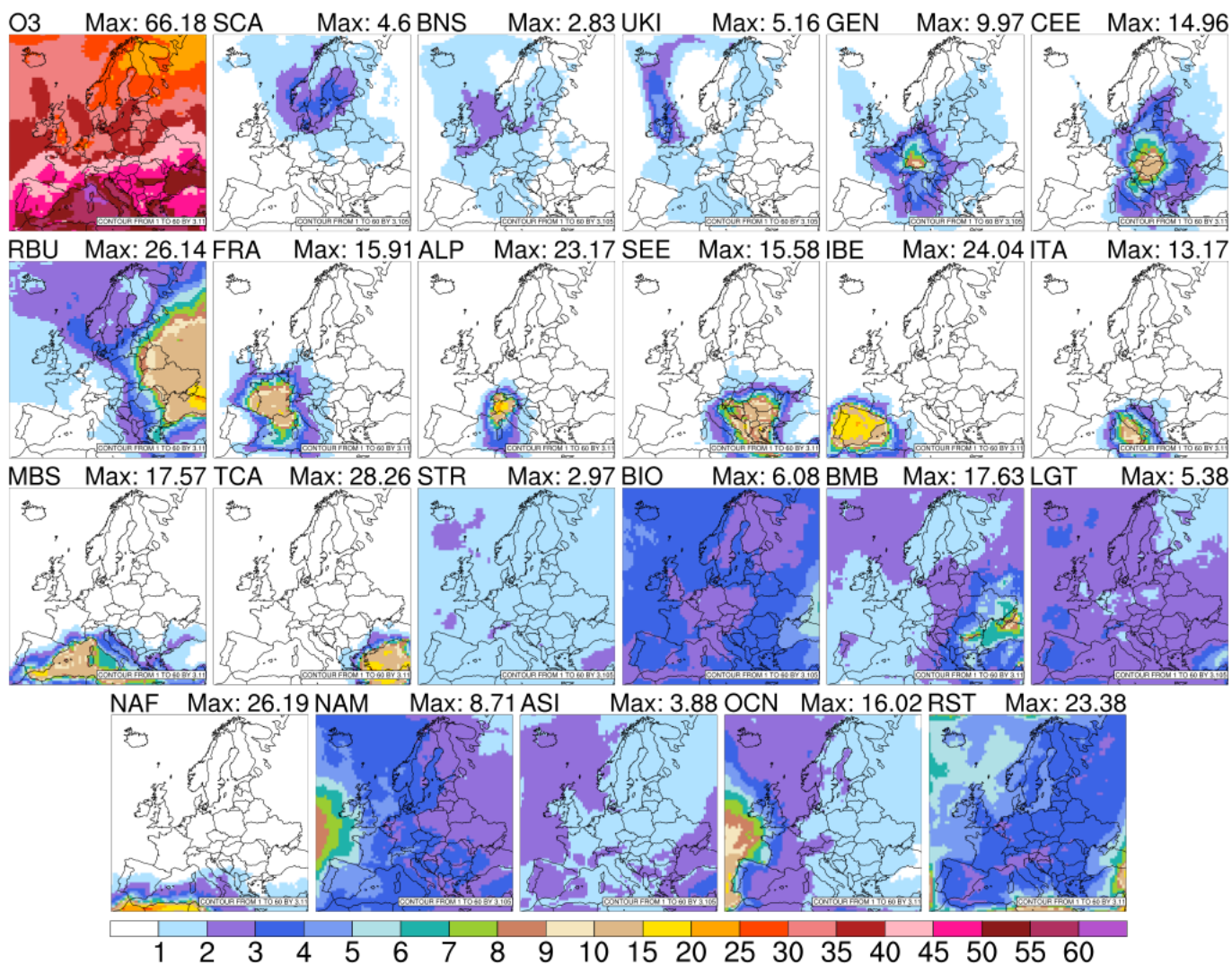
Figure 4. Same as Fig. 2, but for September 2010
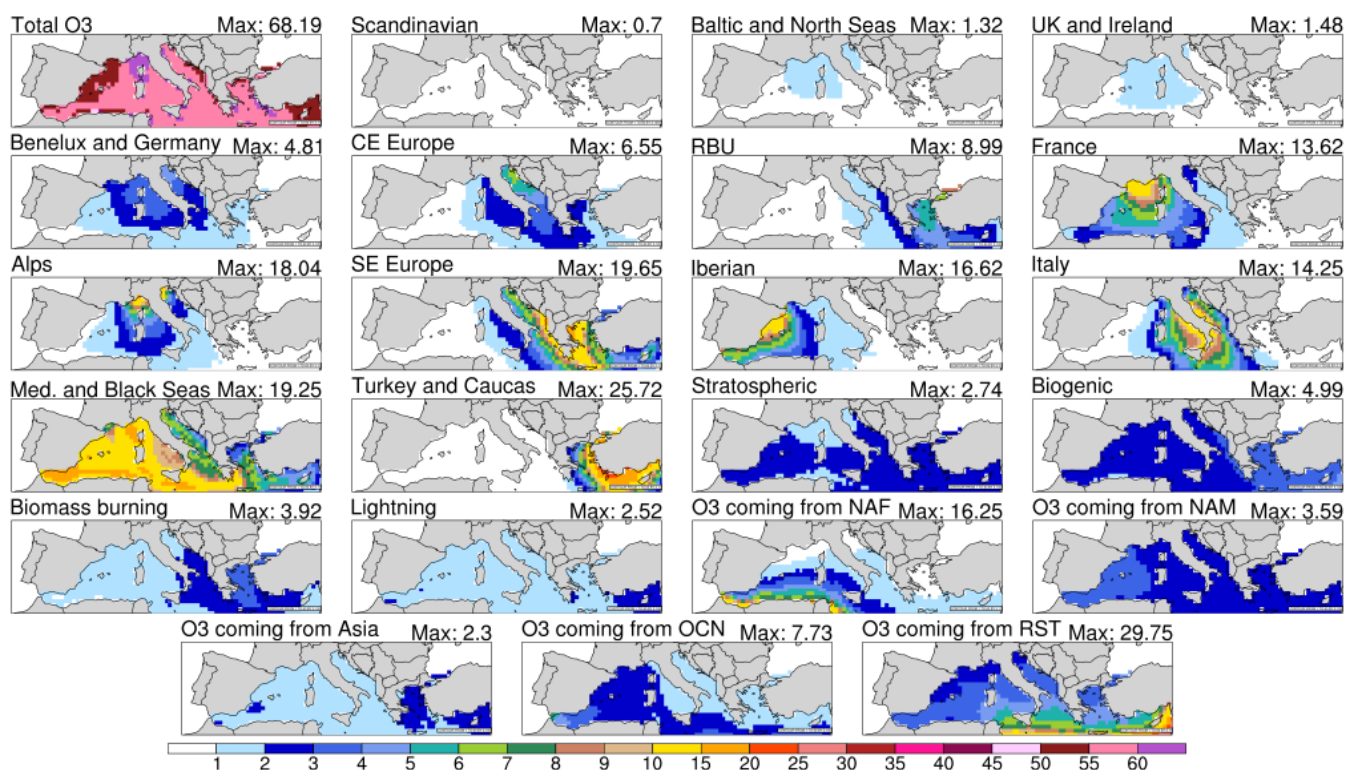
Figure 5. Average MDA8 O$_3$ mixing ratio (upper left panel) and contribution of each tagged O$_3$ region and source over the Mediterranean Sea for the April-September 2010 period. The unit is ppb
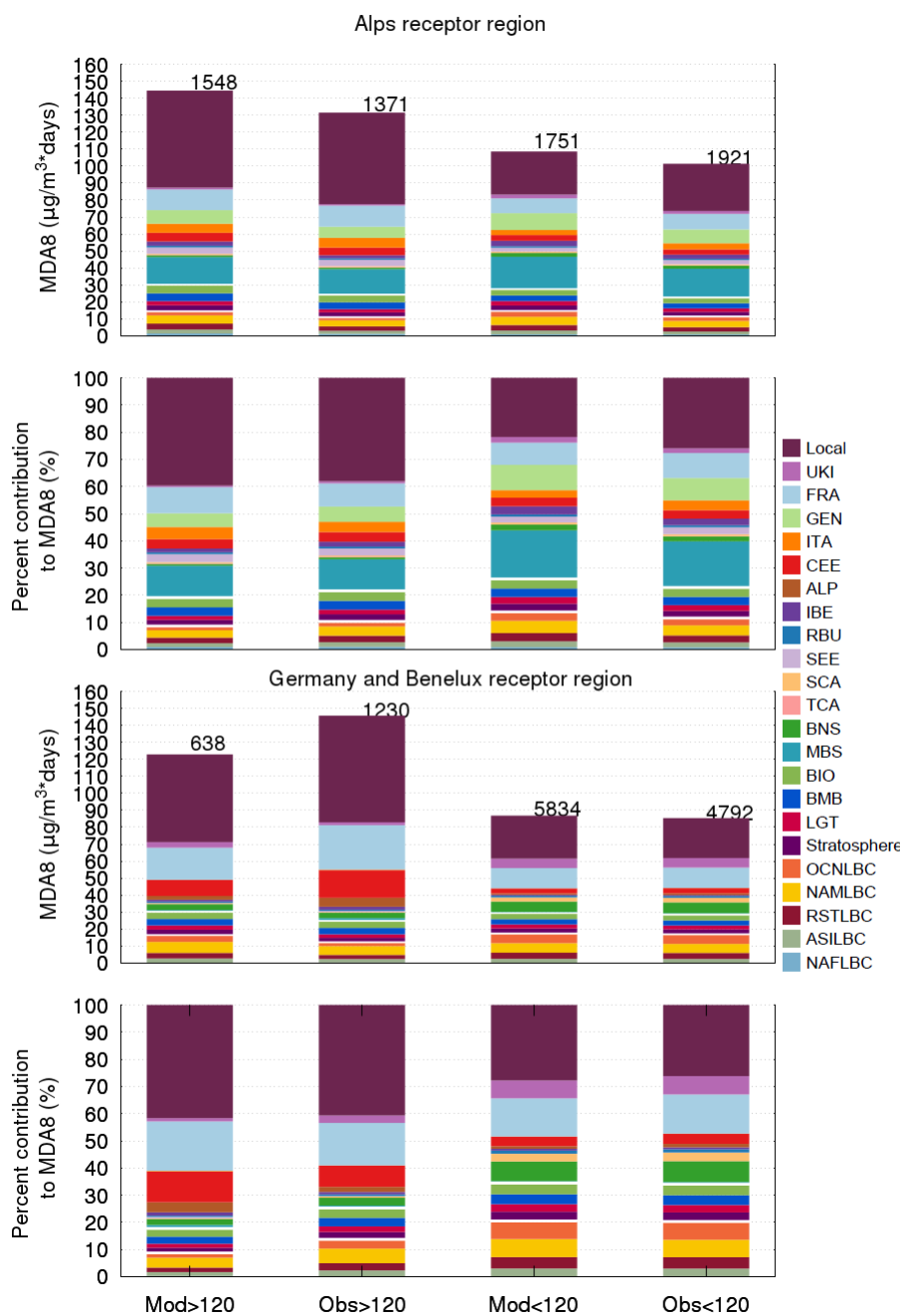
Figure 6. Mean modeled and obseved MDA8 O_3 mixing ratio filtered by a threshold of 120 μ g m^{-}3 for ALP (top panel) and GEN (second from top panel) and percent contribution to MDA8 O_3 from different emissions sources and types for ALP (third from top panel) and GEN (bottom panel) during April-September 2010 period. In each case the contributions of tagged sources to the total O_3 are shown. The tagged contributions to observed O_3 are obtained by scaling the observed O_3 by the relative contributions of these tagged sources to modeled O_3. The total number of exceedances (and non-exceedances) of the MDA8 O_3 target value is indicated at the top of each column
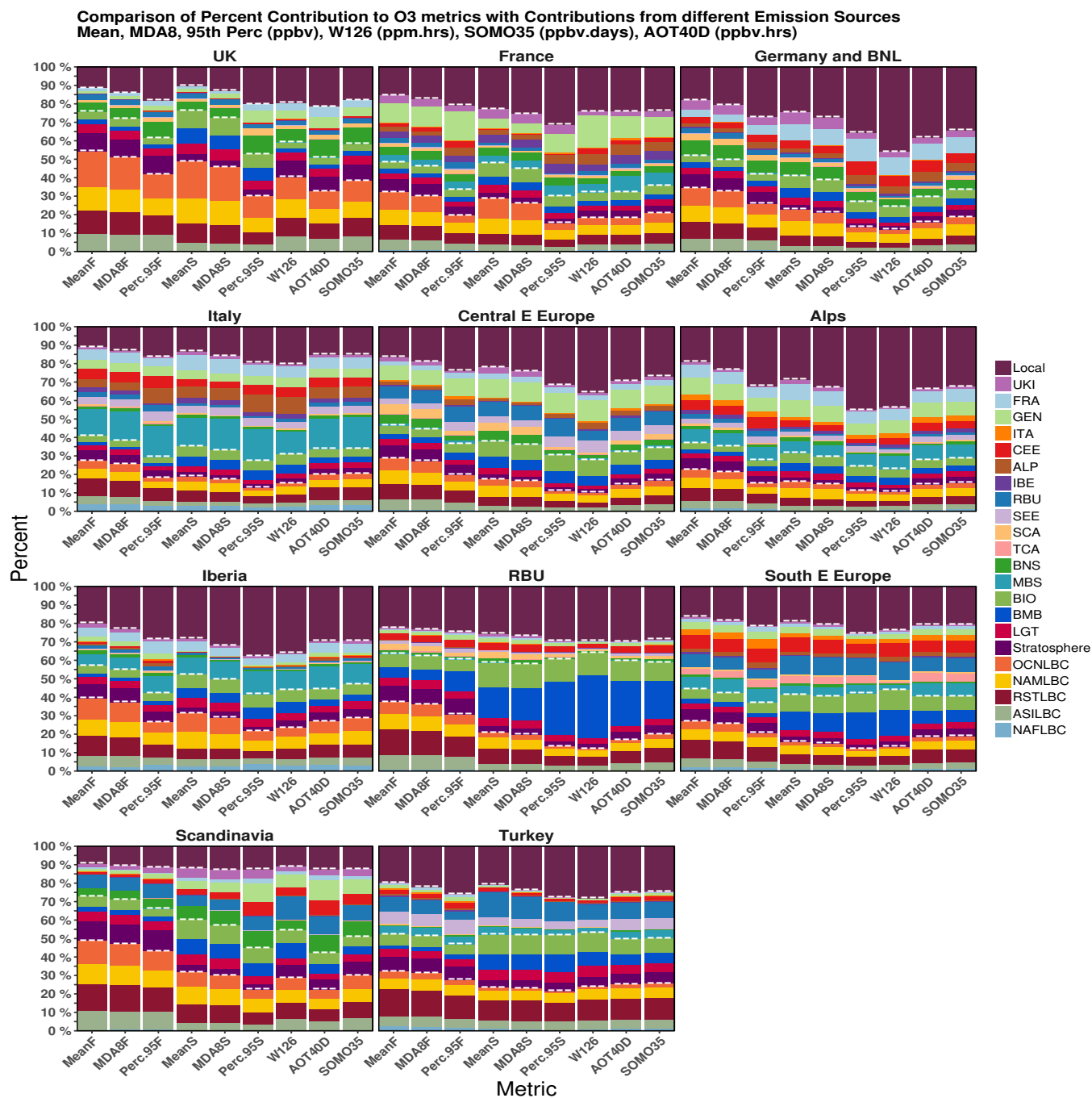
Figure 7. Comparison of percent contribution to O$_3$ metrics from different emissions sources and types. The metrics analysed are mean, MDA8 and 95th percentile ([ppb]) for the early "F" and late "S" simulation period ([ppb]), W126 ([ppm − hours]), SOMO35 and AOT40 ([ppb − hours]). The white dashed lines on each panel separate different categories (intercontinental transport, natural sources, and local and other European sources)
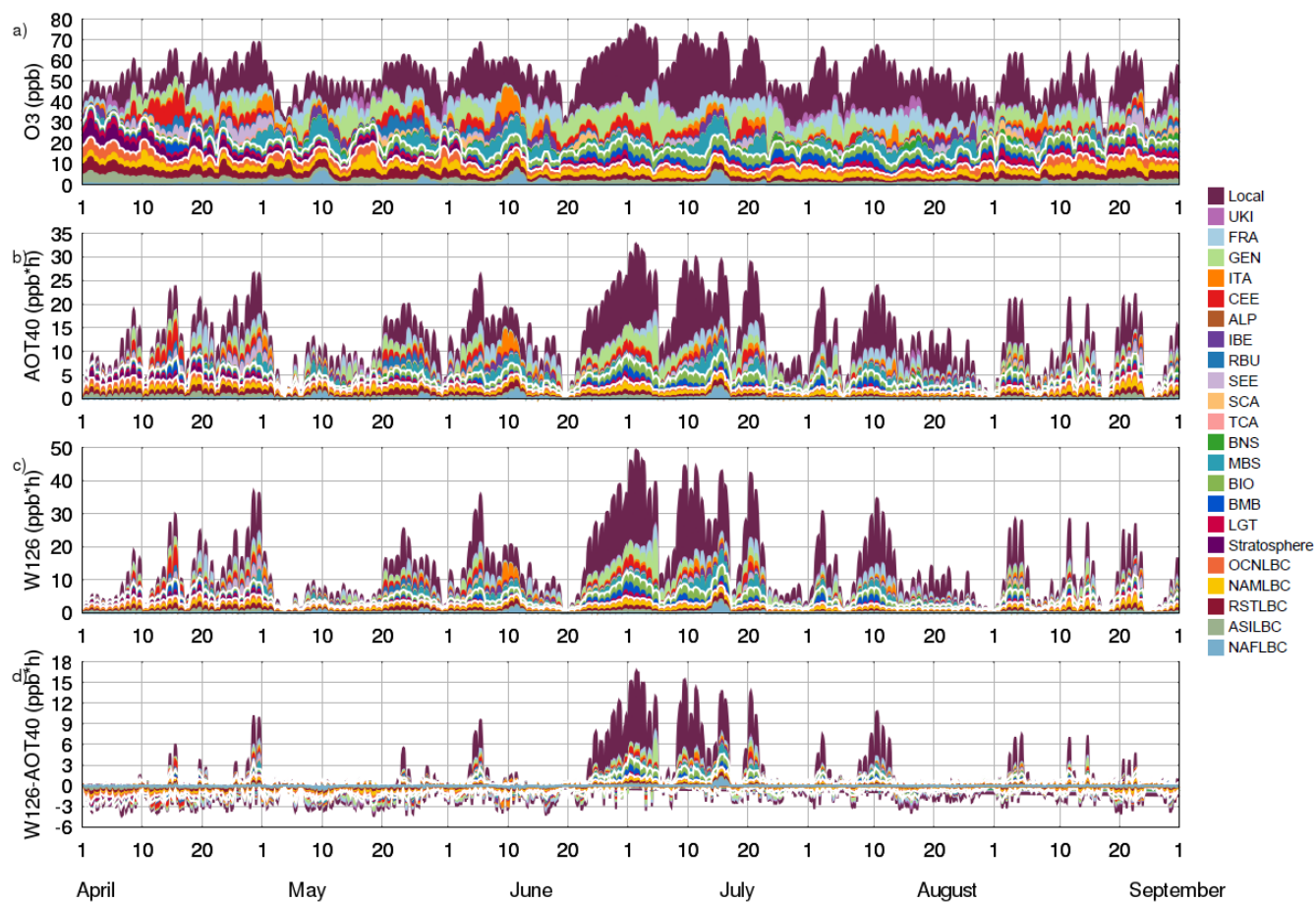
Figure 8. April-September 2010 time series of daytime a) hourly O$_3$, b) hourly AOT40 index, c) hourly AOT40 index and d) differences between W126 and AOT40 indexes averaged over ALP receptor region
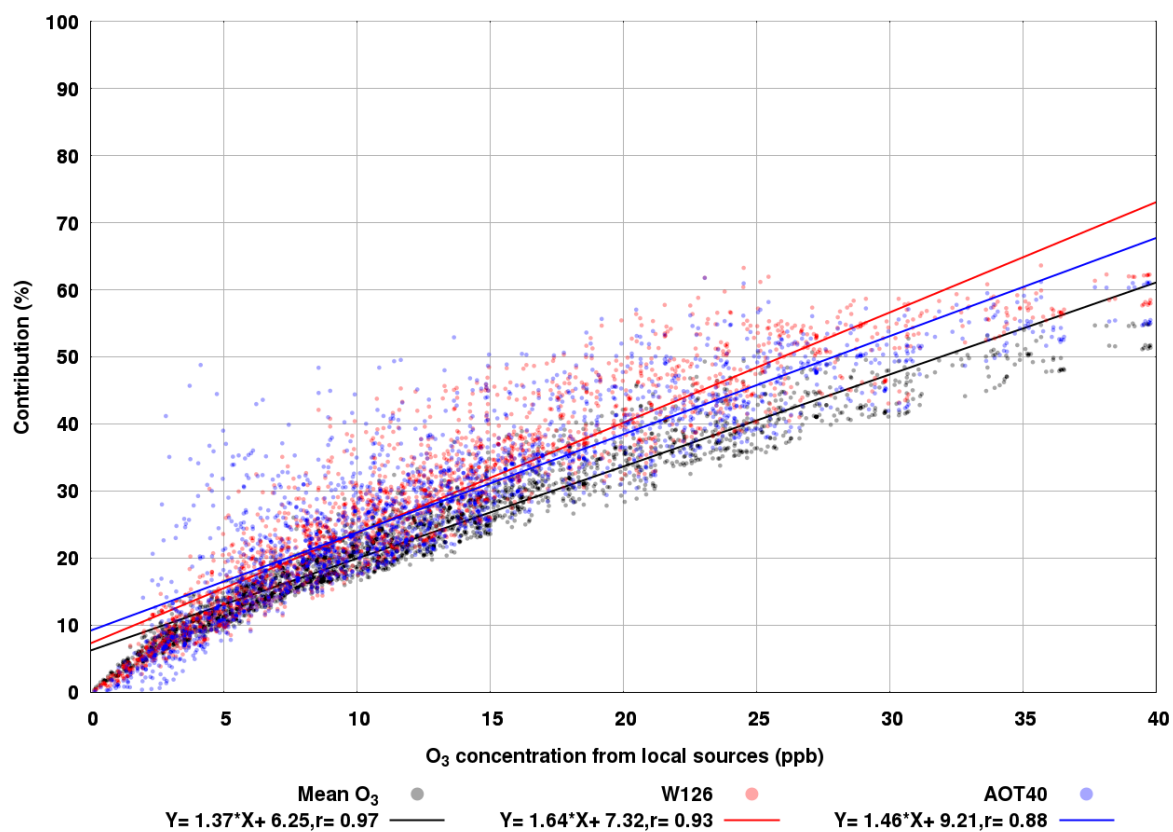
Figure 9. Scatter plots showing the ozone concentration from local sources versus the contribution to Mean O_3 (black dots), W126 (red dots) and AOT40 (blue dots). The solid lines are the lines of best fit.